The actin module of endocytic internalization in *Aspergillus nidulans*: a critical role of the WISH/DIP/SPIN90 family protein Dip1

Marisa Delgado[1,&], Mario Pinar[1,&], Paula Polonio[1,#a], Sergio Fandiño[1,#b], Eduardo A. Espeso[1] and Miguel A. Peñalva[1,*]

Department of Molecular and Cellular Biosciences, CSIC Centro de Investigaciones Biológicas Margarita Salas, Madrid, Spain

[#a] Current address: Department of Biophysical Chemistry, CSIC Insitituto de Química Física Blas Cabrera, Madrid, Spain

[#b] Current address: Department of Animal Health, Faculty of Veterinary, Universidad Complutense, Madrid, Spain

* Corresponding author.
e-mail: penalva@cib.csic.es

[&] These authors contributed equally to this work

30 **Summary**

Using FPs fused with actin or its fiduciary probes Lifeact, Chromobody and Tractin, we studied, by time-resolved microscopy, the actin module of endocytosis in *Aspergillus nidulans*. F-actin probes efficiently labeled endocytic patches and the Spitzenkörper (SPK), but not exocytic cables generated by the SPK-associated formin, illuminated by
35 tropomyosin. The SPK contains actin, tropomyosin and capping protein, but not fimbrin or Arp2/3, showing that the actin mesh in this locale does not contain branched actin. F-actin and its associates Arp2/3, AbpA^{Abp1} and fimbrin reside in patches for 12-14 sec before disappearing. In contrast, verproline resides in patches only during the first half of the actin module, and the scaffold SlaB^{Sla2} arrives long before the burst of F-actin.
40 Hyphal growth depends on endocytic recycling, which we exploited to assess the efficiency of endocytosis in the mutants. *slaBΔ*, *arpC1Δ*, *cof1Δ* (cofilin) and *fimAΔ* (fimbrin) were lethal, with germlings arresting growth shortly after establishing polarity, correlating with a complete block in actin patch progression. *srv2Δ*, *vpr1Δ* (verprolin), *capAΔ* (capping protein alpha) and *dip1Δ* were very debilitating, indicating an important
45 role for these proteins, whereas a double *abpAΔ capAΔ* mutation is nearly lethal. The lifetime of actin in mutant patches correlated with the extent of growth and endocytic defects. Formin does not localize to patches and its deficiency does not affect the F-actin patch lifecycle, ruling out an endocytic role. In contrast, ablation of the WDS (WISH/DIP/SPIN90) Dip1 protein disorganizes tip-proximal patches including the
50 endocytic collar, establishing Dip1-mediated activation of Arp2/3 as a source of seed filaments. However, *dip1Δ* severely impairs endocytosis but does not preclude it, indicating that Dip1-independent preformed seed filaments exist. We document a close association of endocytic patches with cortical actin filaments and abundant traffic of F-actin “worms” that, we propose, might serve as seeds for Arp2/3-mediated dendritic
55 polymerization.

Authors' summary

Filamentous fungi have a deep impact in our lives as friends and foes. Certain species are used as cell factories for the production of proteins or biopharmaceuticals. In contrast, phytopathogenic species, cause important losses in crops whereas those able to infect humans represent serious risks for global health. Filamentous fungi form tubular cells, denoted hyphae, that grow by apical extension. This requires the coupling between exocytosis and endocytosis in the so-called endocytic recycling pathway, which is needed, for example, to maintain the polarization of enzymes which synthesize the cell wall as growth proceeds. Remarkably, detailed studies on endocytosis in filamentous fungi are wanting. Here we report the characterization of the endocytic pathway in the genetic model *Aspergillus nidulans*, a filamentous ascomycete which is well-suited for genetic manipulation and *in vivo* fluorescence microscopy. Our study demonstrates that endocytosis is essential for filamentous fungal life and provides significant insight on how F-actin powers the internalization of endocytic vesicles, including an important physiological role of Dip1, a protein required to provide seed filaments for the formation of F-actin branching networks. Importantly, as yet unidentified Dip1-independent mechanisms that synthesize these seeds must exist, opening new avenues for future research.

Introduction

Pre-synaptic buttons of neurons and hyphal tip cells of filamentous fungi share a distinct subcellular organization. Both are dependent on compensatory endocytosis to recycle membrane and associated proteins that fuse with the plasma membrane at the cellular pole targeted by exocytosis. In synapses, exocytosis occurs at a specialized zone, denoted the active zone, and endocytosis takes place in an area that surrounds that of the active zone [1-3]. in the filamentous ascomycete *Aspergillus nidulans* exocytosis is targeted to the apex, and compensatory endocytosis takes place in a region subtending the apical dome [4-6] Endocytic recycling is crucial for the filamentous mode of life because cell-wall modifying enzymes that are integral membrane proteins polarize by this mechanism [7].

In spite of its basic and applied importance, endocytosis in filamentous fungi has been insufficiently studied. In addition to the intrinsic interest of understanding the fungal mode of life, studies of endocytosis as such are facilitated by three important facts [8]. One is that *Aspergillus nidulans* is a genetically amenable and ideally suited for live microscopy. Second, as endocytosis is essential, mutations impairing this process even to a relatively minor extent translate into a growth phenotype that can be scored by simple growth tests. Third, as integral membrane proteins are efficiently captured by the subapical endocytic collar, mutations decreasing this efficiency permit the unrestrained diffusion of cargoes away from the hyphal tip, thereby providing a highly sensitive test to measure endocytosis [7, 9, 10].

Across the eukaryotic realm, endocytosis occurs in a specialized class of structures – actin patches–, in which endocytic pits develop into cargo-loaded vesicles that are internalized in a process that is powered by a burst of F-actin polymerization involving the Arp2/3 complex [11]. Since the pioneering work of Drubin's and other laboratories, a general model has emerged by which a score of endocytic proteins have been ordered in a pathway that is highly conserved [12-14]. Even though the details of this model have been worked out with notable detail, our understanding of certain aspects of this pathway is insufficient. For example, because the Arp2/3 complex catalyzes the formation of branching actin only on a preexistent actin filament, the proteins required to synthesize these seed filaments are still a subject of debate [15-18].

The process of endocytosis has been studied in filamentous fungal model organisms such as *Neurospora crassa* and *Aspergillus nidulans* [6, 19-26]. However, most of these
115 studies have been purely descriptive and attempts to use the experimental advantages of these fungi to gain insight into the process of endocytosis itself have been scarce. Here we exploit the experimental advantages of *A. nidulans* to study the roles of several endocytic proteins. Deletion alleles of key genes either resulted in lethality or impaired growth markedly, with the strength of impairment roughly correlating with an increase in
120 the time of residence of F-actin in patches and a decrease in the endocytic uptake of cargo, emphasizing the master role of endocytosis in the filamentous fungal mode of growth. Notably, our experiments strongly support the conclusion that formin does not play any role in endocytosis, and that the source of mother filaments that prime Arp2/3 networks is dependent on Dip1. Lastly, our data indicate that Dip1 cannot be the only
125 source of mother filaments, and suggests that this Dip1-independent mechanism might be mediated by cortical actin filaments. Assisted by these data, we propose a model that explains the coupling between the growing tip and the subapical endocytic collar, which was denoted the tip growth apparatus by Oakley et al. [5]

Results

130 Tropomyosin labels both the Spitzenkörper and the actin cables radiating from it

As actin cannot be functionally labeled with GFP, *in vivo* studies of the actin cytoskeleton rely on imaging fluorescent protein-labeled F-actin interactors which serve as proxies. In filamentous fungi, translational fusions of the F-actin-binding oligopeptide Lifeact to
135 fluorescent proteins (FP) have been used in *N. crassa* [27], *A. nidulans* [28] and *Magnaporthe grisea* [29]. Even though FP-Lifeacts display broad specificity, it is well established that certain structures can be visualized only with specific reporters [30, 31]. A remarkable example in *A. nidulans* is the mesh of actin cables radiating from the Spitzenkörper (SPK). The SPK is an accumulation of secretory vesicles localizing
140 underneath the apical plasma membrane that acts as a vesicle supply center [32, 33]. These cables serve as tracks for the myosin-5-dependent delivery of secretory vesicles to the apex [34-37]. Exocytic actin cables have been documented using immunofluorescence microscopy of actin in fixed cells [6, 38]. However, filming these cables *in vivo* has proven to be problematic. The standard reporter used to visualize
145 them is GFP-tagged tropomyosin [39], a protein that plays a key role in the efficacy of myosin-5-dependent transport [5, 40-42]. However, N- and C-terminally GFP-tagged

versions of tropomyosin expressed at physiological levels are not fully functional [5], and we confirmed, using the heterokaryon rescue technique [43], that GFP-tagged TpmA is unable to sustain viability on its own, and therefore that using TpmA-GFP to illuminate
150 exocytic cables requires co-expression of the untagged protein [5]. Recently, the dynamics of tropomyosin cables has been studied after driving expression of N-terminally tagged GFP-TpmA with the *alcA* promoter, but this approach required utilization of 2% (0.22 M) glycerol as carbon source [44]. As we were interested in filming TpmA under more physiological conditions, we set out to develop alternative reporters
155 based on FP-TpmA using two approaches. Firstly, we extended the linker sequence between the tropomyosin C-terminus and the FP from fifteen to eighty residues and used mNeonGreen instead of GFP, as successfully done in *Shizosaccaromyces pombe* [45]. However, this modification resulted in a largely cytosolic localization. Secondly, we constructed a transgene encoding a C-terminal fusion of TpmA to tdTomato (tdT), driven
160 by the *tpmA* promoter. This, and its twin GFP-tagged construct were targeted in single copy to the *white* locus. These two C-terminally tagged TpmAs labeled the mesh of actin cables at the tip, but TpmA-tdT was brighter. Figure 1A shows that TpmA-tdT reveals a 'mop' of actin cables radiating from the SPK that extend basipetally 2-3 μm away from the latter. Remarkably, all reported tropomyosin constructs including ours illuminated the
165 SPK, which strongly indicates that this structure contains a mesh of actin filaments whose organization is similar to that of filaments used for myosin-5 transport

Lifeact labels actin in the SPK, endocytic patches, septa and dynamic actin filaments

Lifeact could modify the dynamics of actin when expressed at high levels. For example,
170 it binds to an epitope on F-actin that overlaps that of the actin filament-severing protein cofilin [46], potentially stabilizing actin filaments. To prevent unwanted effects, we took advantage of the promoter of the *inuA* gene encoding *A. nidulans* inulinase [47] [48]. This gene is inducible by sucrose in a concentration-dependent manner and, unlike most genes required to catabolize alternative carbon sources, is not repressible by glucose,
175 which behaves as a neutral carbon source resulting in low basal levels of expression. By adjusting the carbon source in the culture medium, we were able to tune up expression levels of FP-Lifeact constructs. For example, steady-state levels of Lifeact-GFP obtained on a mixture of 0.05% glucose and 0.025 % sucrose were 10 times higher than those on 1% glucose (Figure 1B). Expression levels of Lifeact on glucose plus sucrose did not
180 affect apical extension rate, which is highly sensitive to perturbations of the actin

cytoskeleton (Figure 1C and supplemental movie 1). Thus, these conditions were routinely used.

GFP and tandem dimer tomato (tdT) versions of Lifeact labelled four different structures, namely contractile actin rings (CARs) at sites of septation, endocytic actin patches, actin filaments, and a bright spot at the position of the SPK (Figure 1D). In contrast to the microtubule cytoskeleton, the actin cytoskeleton is strongly polarized (Figure 2A), mostly as a result of the high abundance of endocytic patches in the subapical collar [4-6]. This collar is located, on average, 1.3 μm away from the hyphal apex and, in two-dimensional projections, defines the base of the apical dome semi-circumference, whose perimeter is, approximately, 4.5 μm (Figure 2B-D and F). Fluorescence intensity indicated that endocytic patches are at least three times more abundant per surface unit in the collar than in regions more distal to the tip (Figure 2B), and maximal intensity projections of time-lapse sequences illustrated they coordinated advance of the endocytic collar and the SPK as hyphae grow by apical extension (Figure 2E).

Co-filming with Lifeact revealed that the plus ends of many microtubules converge at the apex, at the position of the SPK (Figure 2G). Depolymerization of F-actin with latrunculin B dispersed the plus ends of the microtubules across the apical dome, showing the actin-dependence of microtubule organization, whereas depolymerization of microtubules with benomyl resulted in an almost complete disorganization of the endocytic actin collar [5], and the absence of SPK (Figure 2H and I). Both the actin collar and the SPK recovered upon washing out the drug, coinciding with resumption or rapid apical extension and recovery of the normal tip morphology (supplemental movie 2), reflecting the microtubule-dependence of the actin cytoskeleton. This mutual dependence between actin and microtubule cytoskeletons very likely mediates the intimate spatial relationship between the endocytic collar and the growing apex, denoted “the tip growth apparatus” by Oakley and collaborators [5]. Lastly, Figure 2J and supplemental movie 3 show that the organization of the actin cytoskeleton persists during mitosis, reflecting the fact that despite MTs are depolymerized during mitosis to supply tubulin monomers for the mitotic spindle, a subset of cytoplasmic MTs remain stable and suffice to maintain normal rates of apical extension [49] and, as shown by to this experiment, the integrity of the actin cytoskeleton.

215 **Fluorescent protein-tagged actin, anti-actin nanobody and tractin behave as Lifeact**

We wondered if the inability of Lifeact to reveal tropomyosin-containing filaments might be due to artifacts caused by actin regulatory factors competing for binding with Lifeact, and designed an alternative F-actin reporter consisting of a high affinity anti-actin
220 nanobody (chromobody from ChromoTek) [30] fused to either tagGFP2 or mCherry, also expressed under the control of the inulinase promoter. Similar to Lifeact, these reporters did not label actin cables radiating from the apex (Figure 1D). In a further attempt to detect tip cables, we constructed a GFP fusion protein with F-tractin [31], which behaved essentially as Lifeact and nanobody actin reporters (Figure 1D). These data were
225 compared with those obtained with actin, N-terminally tagged with GFP. As numerous reports have concluded that FP-tagged versions of actin are not fully functional, we expressed GFP-actin under the control of the inulinase promoter in a strain backed by a resident copy of the actin gene. GFP-actin was detectable in actin patches, with conspicuous labelling of the endocytic ring, and in the SPK, but it did not label subapical
230 actin filaments or apical cables (Figure 1D and supplemental movie 4). We speculate that the high concentration of actin patches containing branched actin might overcompete cables with regard to the availability of the reporters (see below). We also acknowledge that inability to detect actin cables with high affinity actin-binding domains is consistent with the possibility that these recognize G-actin, and/or nascent filaments,
235 too efficiently, causing steric hindrance with formin and preventing their incorporation into actin cables [30]. In any case, these experiments confirmed, using five different reporters, the presence of F-actin in the SPK and armed us with a set of bright fluorescent fusion proteins that appeared to be well suited to study the dynamics of F-actin in endocytic patches.

240 **Analysis of endocytic patches**

In view of the above results, most experiments described below used the two fluorescent constructs of Lifeact detailed in the preceding paragraph as reporters for F-actin. These were sufficiently bright to permit the acquisition of several minute-long time series with 1-10 fps time resolution, (supplemental movie 5 is Lifeact-GFP at 5 fps). These long
245 periods of illumination did not arrest rapid apical extension, as shown by the tilted lines drawn by the endocytic collar in kymographs traced across the long axis of the hyphae (Figure 3A, this hypha was growing at 1.2 μm/min and filmed at 2 fps). In these plots, the actin-containing phase of each endocytic event was visualized by a more or less vertical line, whose height reflects the time of residence of F-actin in these structures. Even at

250 the 2 fps time resolution used in this experiment, this kymograph clearly illustrates the remarkable number of endocytic events that take place per unit time and reveals that actin patches have static and motile phases, in that order.

We determined that the time resolution that was optimal to analyze these events was 5
255 fps, which is the standard resolution used throughout this work, unless otherwise indicated. Figure 3B shows a typical longitudinal kymograph for a 5 fps Lifeact-GFP time series. The most abundant pattern of actin patch behavior is shown on Figure 3C, top patches, both for GFP- and tdT Lifeact examples. In these patches, actin arrived at cortical structures that remained static for about two thirds of their lifecycle and
260 subsequently underwent short range basipetal and acropetal movements before disappearing from the focal plane. With transversal ROIs, perpendicular to the axis of polarity, kymographs constructed with middle planes showed that F-actin remained cortical up to the end of the patch lifetime, a point at which it appeared to move inwardly and subsequently disappeared (Figure 3C, bottom patches). We chose longitudinal ROI
265 kymographs for a detailed analysis of the patches because transversal kymographs were often difficult to interpret due to the presence of cortical actin filaments that introduced an excessively noisy background. The average residence lifetime of F-actin in patches was 13.7 sec and 13.4 sec with the GFP and the tdT Lifeact reporters, respectively (Figure 3D). Remarkably similar times were measured with chromobody-GFP, F-tractin-
270 GFP and actin GFP, and only a slightly shorter one (11.9 sec) with chromobody-mCh (Figure 3D) (the later minor discrepancy attributable to the highest sensitivity of mCh to photobleaching)

Actin patches associate with filaments and often appear to nucleate them

Z-stack series sharpened with deconvolution algorithms clearly showed actin patches
275 associating with filaments (Figure 4A and B). While estimating the degree of proximity between actin patches and filaments is diffraction-limited, two cases strongly support the contention that patches and filaments are intimately associated. First, association between patches and filaments is observed in essentially every cell. Second, in time-series patches and filaments remain associated across the whole lifetime of the patch,
280 which is difficult to explain if the two structures overlapped by chance (Figure 4C and supplemental movie 6, focused on a long filament). In addition to patches progressing closely associated to filaments, we recorded examples in which filaments appear to be nucleated from patches (Figure 4D). In fact, faint filaments connecting adjacent patches and undergoing cycles of growth and shrinkage can be observed by increasing the

285 contrast of the images. These faint filaments eventually appear to nucleate a neighboring patch (supplemental movie 7). Assuming the correctness of the dendritic nucleation model, we hypothesize that these connections might correspond to filaments that have not yet been severed by cofilin, the said connections becoming more evident under certain mutant conditions (see below).

290

3D (x,y,t) and 4D (x,y,z,t) time series revealed that large pieces of actin filaments are being continually drained away from the tip towards basal regions of the hyphae. These chunks, that we denoted “worms” for its characteristic crawling-like way of movement (supplemental movie 8), result from fragmentation of longer actin filaments, in all 295 likelihood mediated by F-actin severing proteins. Examples of such phenomenology can be clearly seen in the series displayed on Figure 4E, in which a long filament is severed in the middle, the tip-proximal part is depolymerized (shaded in blue) and the tip-distal part moves away from the tip while simultaneously shrinks by its trailing end (shaded in yellow). As this occurs, a new filament (shaded in magenta) grows by its leading end 300 before shrinking by the trailing end. The movement of these actin worms was captured by kymographs, in which they give rise to diagonal lines reflecting their movement away from the tip (Figure 4F). These lines are blurred because the intensity of the signal across minfilaments of actin is not uniform. In the example displayed on Figure 4F, corresponding to a time resolution of 2 fps, several of these mini filaments depart from 305 the tip region, and the parallel diagonal lines to which they give rise in kymographs indicate that they move at approximately 0.4 µm/s. The examples shown on Figure 4G (An x,y,z,t 4D-series corresponding to supplemental movie 9) illustrate that these movements can be considerably long. This movie captures one of these actin microfilaments moving towards the tip, which is exceptional, as in a vast majority of cases 310 they move away from the tip. It also illustrates that length of these runs can be quite considerable. The mechanism propelling these worms is currently unknown (see below), but we note that If these worms moved away from the tip by treadmilling, the leading end of these mini filaments should be the barbed end; which is not compatible with the polarity expected if these mini filaments would have been originated directly by severance of 315 longer filaments nucleated in the apical cortex.

Actin polymerization occurs on SlaB^{Sla2} patches

The burst in actin polymerization reported by the above probes represents the final stages of an endocytic pathway akin to that extensively studied in *S. cerevisiae*, of which we used AbpA^{Abp1} (*i.e.* the homologue of the budding yeast Abp1) as a prototypic

320 component. GFP- and mRFP-tagged AbpA^{Abp1} localize to patches concentrating in the subapical endocytic collar (Figure 5A and supplemental movie 10). In time-lapse series, AbpA^{Abp1} showed the same behavior as F-actin in patches and a time of residence (for AbpA^{Abp1}-GFP) of 13.2 ± 1.7 S.D. seconds (Figure 5B), which is basically identical to that of Lifeact reporters, as expected for a protein belonging to the actin polymerization
325 network. AbpA^{Abp1} is absent from the SPK, further indicating that F-actin in the SPK differs from those in endocytic patches (but see below).

In the budding yeast Sla2 cooperates with Ent1 to couple clathrin-coated endocytic invaginations loaded with cargo to the actin polymerization machinery [50, 51]. The gene
330 encoding *A. nidulans* SlaB^{Sla2} is essential [6, 24]. SlaB^{Sla2} localizes to patches, predominating in the subapical endocytic collar (Figure 5C). With time-lapse acquisitions at 1 fps we determined that the average time of residence of SlaB^{Sla2} in cortical structures is 51 sec +/- 15 S.D., similar to that reported for the budding yeast [12], and notably longer than the time of residence of actin itself (Figure 5D). To demonstrate coupling
335 between endocytic invaginations and the F-actin polymerization machinery, we co-filmed SlaB^{Sla2}-GFP with Lifeact-tdT. Kymographs (Figure 5E) clearly established that the burst in F-actin occurred at the end of the SlaB^{Sla2} cycle, recapitulating the situation in *S. cerevisiae*. Of note, the total time of the cargo selection phase plus the actin polymerization phase is approximately 1 min, like in the budding yeast.

340

Although *slaBΔ* is lethal, a conditional allele driving expression of the protein under the control of nitrate-inducible, ammonium-repressible promoter is available [24]. Conidiospores germinated on ammonium (i.e., without SlaB^{Sla2} expression) arrested growth shortly after establishing polarity, with a characteristic morphology shared by null
345 mutants in every essential gene of the *A. nidulans* endocytic internalization pathway. In these abortive germlings, F-actin appears as characteristic clumps hanging from the cortex (Figure 5F), representing unproductive events of endocytosis due to the uncoupling between the clathrin module and the F-actin polymerization module.

350 Fimbrin is an essential protein present in actin patches and absent from exocytic structures

Another key player in endocytosis is the actin bundling protein fimbrin. In the budding yeast, fimbrin (denoted Sac6) cross-links actin, which appears to be important to generate the force that powers endocytic internalization [12, 52]. Previous work with *fimA*

355 (*A. nidulans* fimbrin), using constructs overexpressing the GFP-tagged protein [4], together with studies with endogenously tagged AbpA^{Abp1} [5, 6] were instrumental to establish the presence of the characteristic subapical endocytic collar. Figure 6A shows the distribution of endogenously tagged fimbrin-GFP, which is present in patches that are markedly concentrated in the subapical collar. Notably, these experiments revealed
360 that, unlike actin, fimbrin is absent from the SPK. Figure 6B illustrates the behavior of *fimA*-GFP in these patches, with a time of residence of 13 +/-1.07 sec S.D. which, like its motility behavior, matches that observed with actin reporters described on Figure 3.

S. cerevisiae fimbrin, encoded by *SAC6*, plays a key role in endocytic patches by cross-
365 linking F-actin filaments of the dendritic network [52]. Somewhat unexpectedly, an *A. nidulans* disruption mutant of *fimA*, *fimA::Tn341*, in which the open reading frame had been interrupted by transposon mutagenesis, was viable [4], even though it formed morphologically abnormal hyphae and showed delayed polarity establishment. On Figure 6C we show, using Lifeact-GFP, that *fimA::Tn341* disorganizes the endocytic
370 internalization collar and prevents the localization of F-actin to the SPK, illustrating the intimate coupling between exocytosis and endocytosis. Given that ablation of key endocytic proteins such as Rvs167, SlaB^{Sla2}, components of the Arp2/3 complex or cofilin is lethal [[6, 24] and this work], we hypothesized that *fimA::Tn341* was a partial loss-of-function allele. The growth test on Figure 6D shows that whereas a *fimA::Tn341* strain is
375 severely debilitated but able to grow to a certain extent, a strain carrying the complete deletion allele of *fimA* is unable to grow, strongly indicating that *fimA::Tn341* is not a null allele. To confirm this conclusion we studied the terminal phenotype of *fimA*Δ using the heterokaryon rescue technique [43]. We constructed a heterokaryotic *fimA*Δ/*fimA*+ strain by transformation, from which we obtained homokaryotic *fimA*Δ conidiospores. These
380 conidiospores were able to establish polarity and to maintain it for a limited time before arresting growth with a characteristic shape that is shared with mutants completely deficient in endocytosis (Figure 6E and supplemental movie 11). In these abortive germlings, F-actin accumulated in bright spots at the periphery that did not progress any further. Thus, the complete absence of fimbrin abolishes F-actin dynamics to an extent
385 that is incompatible with viability, and *fimA::Tn341* is a partial loss-of-function allele.

We exploited this allele to determine, using time-lapse microscopy, the behavior of endocytic patches labeled with Lifeact-GFP when *fimA* is compromised. Impairing *fimA* function had to notable consequences. Firstly, actin was recruited to patches, but the
390 lifetime of actin patches augmented to 27.6 sec +/-5.4 S.D., *i.e.* approximately twice that determined for the wild-type (Figures 6F and 7). In addition, patches were static,

completely lacking any motile phase, as reflected by kymographs (Figure 6F, top and bottom left) and time-lapse movies (supplemental movie 12). We conclude that proper cross-linking by fimbrin is required by dendritic actin in endocytic patches to power a
395 productive endocytic event.

Cofilin is essential

Cofilin is the main F-actin severing protein in eukaryotic cells [53, 54]. Deletion of *cof1*, the only gene encoding cofilin in *A. nidulans* (AN2317) is lethal (Figure 8A). Haploid *cof1Δ* conidiospores, obtained from heterokaryons, establish polarity before arresting
400 growth with a typical terminal phenotype of endocytosis-less mutants (Figure 8B), with F-actin accumulating in cortical patches that do not progress any further (Figure 8C). Cof1-GFP appears to be lethal, but we could rescue the corresponding gene in diploids carrying a backup copy of the wild-type allele. In these heterozygous diploids, cofilin localizes to patches, highly enriched in the endocytic ring (Figure 8D). The lifetime of
405 cofilin in these patches was 20 +/- 4.4 s S.D. (supplemental Figure 1).

Endocytic role of suppressor of RAS valine (Srv2)/cyclase associated protein (CAP)

As cofilin is essential and we wanted to test the effects of impaired actin turnover, we targeted one of the components of the complementary mechanism for disassembling
410 actin filaments, which is mediated by Srv2/CAP and twinfilin. Srv2/CAP dramatically accelerates depolymerization of actin filaments at their pointed ends [55, 56]. In *Aspergillus*, ablation of Srv2/CAP (AN0999) markedly impairs colony growth (Figure 9A), as expected for a gene playing an important role in endocytosis. Indeed, Lifeact-GFP imaging revealed that *srv2Δ* disorganizes the normal distribution of actin patches such
415 that either they no longer assemble into a collar or they gather in a collar assembled far away from the apex (Figure 9B and supplemental Figure 2). Kymograph analysis of movies acquired at 5 fps revealed that *srv2Δ* results in patch lifecycles that double in duration the wild-type (Figure 7), although these patches still transited through static and motile phases (Figure 9C). A useful estimation of the degree to which endocytosis is
420 prevented by any given genetic intervention is determining to what extent is the efficiency of the endocytic collar impaired. This may be achieved by measuring the polarization of protein cargo that becomes polarized by endocytic recycling [7, 57]. In the wild type, endogenously tagged chitin synthase B (ChsB, an integral membrane protein) localizes to the SPK and to the apical dome plasma membrane, reaching, on average, a distance
425 of approximately 2 μm from the apex before being internalized by the endocytic collar. In

this ChsB endocytic recycling assay, *srv2Δ* severely impaired this efficiency (Figure 9D). Thus, Svr2 is required to determine the normal duration of the actin burst during endocytic internalization and to maintain the coupling of the endocytic collar to the growing tip.

430

As endogenous tagging of the protein is debilitating, indicating incomplete function (Figure 9A), the behavior of Srv2-GFP was uninformative, beyond the observation that it is able to localize to cortical patches (supplemental Figure 2). These Srv2-GFP patches had a lifetime longer than one minute, and underwent short-distance movements similar
435 to those observed with Cof1-GFP (supplemental Figure 2 shows kymographs comparing Srv2-GFP to Lifeact patches).

Once the involvement of Srv2 in endocytosis had been determined, we proceeded to analyze the effects of its ablation on the dynamics of actin. Time-lapse movies of Lifeact
440 in *srv2Δ* cells revealed the appearance of bright actin structures that often connected patches localizing to opposite sides of the hyphae (Supplemental movie 14), supporting the notion that F-actin disassembly is indeed deficient in *srv2Δ* cells. These movies also revealed the presence of cortical structures that moved basipetally and gave rise to "worms", akin to those observed in the wild type, but which were conspicuously more
445 abundant in the *srv2Δ* mutant (supplemental movie 15). Movies additionally showed that these worms originated at actin patches (supplemental movie 16) and that they traveled for several micron-long distances before being depolymerized (supplemental movie 17; supplemental Figure 2). In the example shown on Figure 9E one such worm was filmed leaving behind a tail of F-actin that resembles that left by *Listeria* cells (readers should
450 also consult supplemental movie 17). Depolymerization of these worms took place from the tip proximal pole, suggesting that this pole represents the barbed end of filaments originating at endocytic patches (depolymerization by the pointed end was predictably impaired by the absence of Srv2). The interpretation that the tip-proximal (lagging) end is the barbed end implies that this movement cannot be attributed to treadmilling, which
455 would require the opposite polarity.

Arp2/3 mediates actin polymerization in endocytic patches but is absent from exocytic actin structures

The burst of F-actin polymerization driving endocytosis reflects the formation of branched actin networks synthesized by the Arp2/3 complex [14, 58]. Hyphal tip growth might
460 resemble expansion of the cytoplasm during the protrusion of filopodia of higher cells,

which is also driven by Arp2/3 [53]. To study the possibility that branched actin is involved in tip growth, we tagged endogenously the ARPC5 and ARPC1 (AN5778) subunits with GFP (for Arp2/3 we will use *S. pombe* nomenclature). *arpC5-gfp* resulted in lethality (data not shown), as did *arpC1*Δ (Figure 10A). *arpC1*Δ spores collected from heterokaryons
465 arrested growth with the characteristic morphology of abortive germtubes unable to maintain polarity (Figure 10A, boxed). In contrast, *arpC1-gfp* strains are viable and Figure 10B shows that endogenous GFP tagging of ArpC1 does not affect colony growth, indicating that the fusion protein is functional. ArpC1-GFP is present in patches akin to those labeled by chimeric actin reporters (Figure 10C)(supplemental movie 18). The
470 lifetime of ArpC1 in these patches was 13.9 sec +/– 1.9 S. D. (Figure 10D), which matches those of $AbpA^{Abp1}$ and Lifeact. Indeed, the lifecycles of ArpC1-GFP and Lifeact-tdT were essentially indistinguishable (Figure 10E and F), in agreement with the fact that the burst in actin polymerization driving endocytosis is catalyzed by Arp2/3.

475 A key observation was the complete absent of Arp2/3 at the position of the SPK. This finding is important because it implies that the mesh of actin present in this structure is not branched actin. To buttress this key conclusion further, we used fluorescent versions of the SPK residents MyoE (myosin-5) and SepA (formin). Figure 11A shows that MyoE is present in a narrow a spot at the apex [59] , whereas vesicles that arrive at the tip by
480 the endocytic recycling pathway, labeled with the endocytic tracer FM4-64 [23, 60], show a slightly wider distribution, overlapping that of the secretory vesicle marker Rab11 [36, 61]. Myosin-5 is a barbed end-directed motor that in the steady-state accumulates at the SPK because SepA, the only *A. nidulans* formin, nucleates actin filaments with their barbed ends at the SPK [5, 39, 59, 62]. To get a robust signal of SepA, we labeled this
485 protein endogenously with a triplicated GFP. Myosin-5 colocalizes strictly with the formin in the apices of hyphae (Figure 11B). validating it as SPK marker. Figure 11C is a confocal image showing that Arp2/3 is completely absent from the hyphal dome, restricting its localization to the endocytic collar, whereas MyoE is completely absent from the endocytic collar, restricting its localization to the SPK. Thus, the SPK does not
490 contain branched actin.

Verprolin plays an important role early during the F-actin lifecycle, being required for the transition between motile and non-motile phases.

Verprolin coordinates the NPF activities of WASP/Wsp1 and type I myosin during Arp2/3-mediated branched actin polymerization [63-66]. While its interacting network has been
495 studied, its physiological role is insufficiently understood. There is a single verprolin

homologue in *A. nidulans*, encoded by *vpr1* (AN1120). Ablation of Vpr1 results in a marked inhibition of growth, consistent with it playing an important role in endocytosis (Figure 12A). We verified that endogenous C-terminal tagging of Vpr1 does not impair function before analyzing its localization and dynamics. Vpr1-GFP localizes to actin
500 patches/endocytic collar but is absent from the SPK (Figure 12B), further indicating that this structure does not contain branched actin. The average time of residence of Vpr1 in these patches is 8.1 +/- 0.8 sec (S.D), which is markedly shorter than that of Arp2/3 (Figure 12C). Dual color imaging established that Vpr1 is recruited to patches on the first half of the Arp2/3 lifecycle, during the non-motile phase (Figure 12D). Supplemental
505 movie 19 shows that Vpr1-GFP is recruited to actin patches with ArpC1-mCh and disappears from them before actin patches transit from the non-motile to the motile phase.

Kymograph analysis of Lifeact patches revealed two interesting observations: one is that
510 the absence of Vpr1 completely abrogates the motility of actin patches across the whole F-actin cycle, indicating that it is required for the transition from the non-motile to the motile phase (Figure 12E). The second, that the absence of Vpr1 extended the lifecycle of F-actin to 25.7 +/- 4.1 sec (S.D.) (Figure 7 and 12F), approximately doubling the lifetime in the wild type. So, Vpr1 plays an important role in generating the branched actin
515 network that powers endocytic internalization. In the endocytic recycling assay, ChsB was markedly depolarized in the *vpr1Δ* background, diffusing across the plasma membrane up to 15 µm away from the apex, in sharp contrast to the wild-type, in which ChsB extended for *circa* 2 µm (Figure 12G). Therefore, this functional analysis combined with growth tests and studies of F-actin residence in endocytic patches underline the key
520 importance that verprolin plays in endocytosis by regulating F-actin dynamics.

*abpA*Δ and *capA*Δ show a strong synthetic negative interaction in growth and endocytosis

Several physiological systems curb F-actin polymerization. *capA* (AN2126)[67] encodes the alpha subunit of capping protein, which in Arp2/3 networks restricts the addition of
525 actin subunits onto the barbed ends of actin filaments [12, 68], arresting polymerization. Ablation of capping protein results in only mild endocytic defects, and it has been reported that in the budding yeast this results from the existence of an alternative pathway mediated by Aim3 and Abp1, such that the simultaneous absence of both systems makes the endocytic defect severe [68]. We set out to study this mechanistic
530 redundancy in *Aspergillus*, taking advantage of the key role of endocytic recycling in

hyphal growth. AbpA-GFP localizes to the endocytic collar but not to the SPK, indicating that it plays no exocytic roles (Figures 5A and 13A). With regard to its role in endocytosis, *abpAΔ* strains have no growth defects [5, 6], whereas *capAΔ* strains display a marked impairment of growth (Figure 13B), attributable, in part, to its endocytic role, but also to
535 its anticipated role in the regulation of non-endocytic F-actin structures, such as filaments/cables emanating from the SPK. Indeed, *capAΔ* (but not *abpAΔ*) delocalizes F-actin from the SPK (Figure 13C) and GFP-tagged CapA labels this structure strongly (Figure 13D). It should be noted that endogenous GFP-tagging of CapA results in a slight growth defect at 25-30°C (endocytic assays were carried out within these temperature
540 limits), which becomes conspicuous at 37° (supplemental Figure 3). Despite this caveat, CapA-GFP localizes to endocytic patches, but the time of residence of CapA-GFP is 27.3 +/- 8.7 sec (S.D.) (supplemental Figure 3), which doubles that of F-actin. Because capping protein is expected to overlap largely with the lifecycle of F-actin, this long time of residence almost certainly reflects impaired function of the fusion protein. The
545 debilitating effect caused by *capAΔ* is strong, but does not compromise viability. The endocytic collar often invades the apical dome and it is less densely populated by actin patches, with frequent intermingling of actin tails originating from patches located on opposite sides of the hyphae, suggestive of unrestrained actin polymerization (supplemental movie 20).

550

In sharp contrast with *abpAΔ* and *capAΔ* single mutants, the double mutant is severely debilitated (Figure 13B and E), indicating that CapA and $AbpA^{Abp1}$ share a nearly essential function. *capAΔ* impaired the F-actin cycle in patches, nearly doubling the time of residence in the wild-type (from 14.8 sec to 23.7 +/- 5.6 sec (S.D.)(Figure 7).
555 Combining *capAΔ* with *abpAΔ* resulted in a further increase in Lifeact time of residence to 34.2 +/- 5.6 sec (S.D.) (Figure 7). Thus, the time of residence of Lifeact in patches correlates inversely with growth, strongly indicating that an increase in this parameter reflects a larger defect in endocytosis. We validated this conclusion by determining the effects of the mutations on the endocytic recycling of GFP-ChsB. These experiments
560 (Figure 13E) demonstrated that endocytosis is essentially normal in the *abpAΔ* single mutant, significantly less efficient in the *capAΔ* single mutant and severely debilitated in the *capAΔ abpAΔ* double mutant. In agreement with this marked defect in endocytic recycling, *capAΔ abpAΔ* hyphae displayed recurrent losses of polarity, abnormal hyphal morphogenesis, major disorganization of the actin cytoskeleton, ectopic septation and
565 lack of progression of actin patches (supplemental Figure 3)(supplemental movie 21).

Formin is not required for the biogenesis of endocytic F-actin

Because the Arp2/3 complex is unable to nucleate new actin filaments without a mother
570 filament that serves as seed for the formation of branches, there must be a mechanism/mechanisms ensuring that the priming filament is assembled at, or recruited to the sites of endocytosis. This aspect of the biogenesis of actin patches is insufficiently understood in general and has never been investigated in filamentous fungi. It has been argued that this mother filament will be provided by formin synthesizing such a filament
575 *de novo* at endocytic sites. However, the single *A. nidulans* formin, SepA, localizes to the SPK and to contractile rings, but has not been detected in the position of the endocytic collar, despite the high density of actin patches that it contains [39, 69, 70]. As it could be argued that this lack of detection is due to the low abundance of this protein in the cell, we decided to address this problem genetically, exploiting *sepA1*, a heat
580 sensitive mutation in *sepA*, which inactivates function at 37°C and higher (supplemental Figure 4). Indeed, whereas the localization of actin and the SPK was not affected by shifting wild type cells to 37°C for three hours, the signal of actin at this locale was completely lost when *sepA1* cells were filmed instead (Figure 14A). Under these conditions, the average lifetime of Lifeact in endocytic patches was essentially
585 indistinguishable at 28°C or 37°C, irrespective of whether cells were wild type or carried the *sepA1* mutation, strongly arguing against involvement of SepA in endocytosis (Figure 14B). To buttress this conclusion, we repeated similar experiments using endogenously tagged FimA-mCh, which led to the same conclusion (Figure 14C). We conclude that formin is not required to provide mother filaments that prime Arp2/3-mediated synthesis
590 of branched actin networks during endocytosis.

Dip1 funnels actin towards endocytic patches

In view of this lack of involvement of formin, we turned our attention to the *Aspergillus* homologue of Dip1, a member of the WDS (WISH/DIP/SPIN90) family of proteins. Unlike WASP and other NPFs that recruit Arp2/3 to the sides of preformed actin filaments, Dip1
595 binds and activates Arp2/3 without a pre-existing mother filament, remaining bound to the nascent linear filament by Arp2/3 [15-17, 71, 72]. Endogenously GFP-tagged Dip1 is functional (supplemental Figure 5) but weakly fluorescent. Dip1-GFP localizes to actin patches (Figure 15A), in agreement with its predicted role in endocytosis. Ablation of Dip1 results in a conspicuous growth defect, but *dip1Δ* cells are viable, indicating partial
600 functional redundancy with other pathways (Figure 15B). *dip1Δ* does not affect the localization of the SepA formin nor the accumulation of F-actin in the SPK (Figure 15C and D), yet *dip1Δ* dramatically facilitated the visualization of Lifeact-labeled actin

filaments/cables in the tips, which now were very conspicuous (Figure 15D, E and F; supplemental Figure 5). Inspection of images immediately provided a plausible
605 explanation: actin patches appeared to have been removed from the tip proximal regions and the endocytic collar was completely absent, which on the one hand facilitates detection of filaments without the strong background of actin patches and on the other very likely enlarges the pool of G-actin available for linear F-actin structures [73]. Kymographs revealed two additional pieces of information; one was that Lifeact
610 residence time in patches nearly doubled the wild-type (23 vs. 14 sec, Figure 7 and 15G); the second, which has significant implications for any model of the actin cytoskeleton in *Aspergillus,* is that a remarkable flow of actin filaments departing from the SPK towards basal regions of the hyphae, which appear as tilted lines originating at the apex, was very noticeable (Figure 15F). Supplemental movies 22 and 23 demonstrate that these
615 represent filaments of actin that are continuously emerging from the SPK, synthesized by SepA formin. This observation will be taken over in the discussion. Lastly we confirmed, using FimA-GFP, that the average lifetime of actin patches was faithfully reflected by Lifeact, as these experiments gave rise to fully consistent values (26 vs. 14.7 sec in the mutant vs. the wild-type) (Figure 15H and I). The key role that Dip1 appears
620 to play in endocytosis was confirmed using endocytic recycling assays of chitin synthase B, which showed that the distance to which this transmembrane cargo diffuses away from the tip in *dip1Δ*, cells is the highest among any other mutant tested (Figure 15K). Endocytic recycling and hyphal tip growth are intimately related, and therefore it should come as no surprise that the apical extension rate of *dip1Δ* is reduced by half relative to
625 the wild-type (supplemental Figure 5). The relative ease with which actin filaments were detected in *dip1Δ* cells permitted the visualization of numerous actin patches that appeared to be captured by actin filaments, but, most importantly, of numerous patches that were being formed in close vicinity to these filaments (Figure 15J). Given that there must be a mechanism to provide mother filaments for Arp2/3 that is independent of Dip1,
630 we should like to propose that these cortical actin filaments provide sites on to which Arp2/3 networks can be built up to propel endocytic invaginations into the cytoplasm. A slightly different version of this model, denoted “touch and trigger” was originally proposed by Pollard and co-authors for *S. pombe* [74].

Discussion

635 The process of endocytosis is intimately associated with the mode of life of filamentous fungi, which form long tubular cells, denoted hyphae. Hyphal tip growth is crucially dependent on the polarization of cell wall modifying enzymes, which is mediated by

endocytic recycling [7, 36]. Therefore, hyphal tip cells are arguably among those which are most dependent on endocytosis for viability. Studies in the budding and in fission
640 yeasts have revealed the involvement of a highly conserved pathway in which different protein modules act sequentially to drive invagination of the primary endocytic vesicle against internal turgor [12]. Parallel work with metazoan cells revealed that the core machinery is strongly conserved across the lineage that includes fungi and Metazoa [14]. Remarkably, in spite of the applied interest of filamentous fungi as producers of enzymes
645 and metabolites, or of their clinical interest as devastating pathogens, the process of endocytosis has been insufficiently studied even in model organisms such as *N. crassa* and *A. nidulans*. One of the aims of this study is to fill this gap, approaching endocytosis as one of the major physiological functions of the actin cytoskeleton. A second study on the role of F-actin in exocytosis will be reported elsewhere.

650

We used three different parameters to determine the extent to which a genetic intervention impairs endocytosis. One was the time of residence of F-actin in endocytic patches. The second was the colony phenotype because, due to the role of endocytosis in hyphal growth, the greater the impairment of endocytosis is, the more debilitating that
655 the causative mutation becomes for colony growth. The third was the efficiency of polarization of the chitin synthase ChsB, a model cargo which is a substrate of the endocytic recycling pathway. The time of residence of F-actin in patches was determined with a time resolution of 0.2 seconds using Lifeact, chromobody and tractin, tagged with FPs. This parameter was highly reproducible in the wild-type, independently of the probe
660 and FP used, with an average value of 13-14 seconds at 25-28°C. Of note, endogenously FP-tagged proteins belonging to the actin module showed consistent lifetimes (of 13.2, 13.1, 13.9 and 12.9 sec for $AbpA^{Abp1}$, FimA , ArpC1 and actin, respectively) buttressing this conclusion. In contrast, each and every mutation that had a negative impact on colony growth extended the time of residence of actin in patches in a roughly
665 commensurate manner, with the largest value (34 sec) resulting from the severely debilitating synthetic negative interaction between *capA*Δ and *abpA*Δ, predictably reflecting a marked deficit in barbed end capping activity. *srv2*Δ*, dip1*Δ, *vpr1*Δ, and *capA*Δ, which resulted in less severe colony growth defects, showed F-actin resident times approximately doubling the wild type. *fimA*Δ*, arpC1*Δ*, slaB*Δ and *cof1*Δ resulted in
670 lethality. Spores carrying a lethal mutation can be rescued in heterokaryosis and allowed to germinate until they reach a terminal phenotype. In all these three cases, mutant strains were able to establish polarity but arrested growth shortly after that, with a yeast-like phenotype that resembles the already described *slaB*Δ phenotype [6], undisputedly establishing that endocytosis is required to maintain polarity during hyphal tip growth. It

675 is worth noting that F-actin can form cortical structures even in the absence of the Arp2/3 complex.

The lethal phenotype of *fimA*Δ deserves separate consideration, because it served to establish that the previously described *fimA::Tn341* mutation [4] is not a complete-loss-
680 of-function allele, which was instrumental to reveal that when fimbrin is compromised, F-actin patches do not transit from the non-motile to the motile phase, a phenotype that this mutation shares with *vpr1*Δ. Vpr1 has been reported to regulate NPF factors, and we show here that it arrives to patches at the beginning of the F-actin cycle.

685 An important observation was that actin patches frequently overlapped with actin filaments. This overlap appears to result, on the one hand, from the biogenesis of these structures in close association with cortical filaments, whereas in other examples patches appeared to give rise to small filaments that eventually underwent basipetal movement, forming moving structures that we have denoted “actin worms”. These worms were
690 clearly noticeable in the wild type, but became very conspicuous in the *srv2*Δ mutant. That these worms stem from patches and move mostly in basipetal direction strongly suggests that the leading end is the pointed end of these filaments, and therefore that these worms do not move by treadmilling. In any case, the close association of patches and filaments would be consistent with the latter serving as seeds for the Arp2/3
695 complex-mediated burst of actin polymerization, as suggested [74]. This possibility led us to consider the origin of the seed filaments which are required by Arp2/3. *A. nidulans* has a single formin, SepA, which does not appear to play any role in the organization of the endocytic collar or in the duration of the actin phase of the endocytic cycle, making its participation in the process very unlikely. Thus, we explored the implication of the
700 WISH/DIP/SPIN90 family protein Dip1. Strikingly, ablation of this protein resulted in major changes in the organization of the actin cytoskeleton. Firstly, the endocytic collar was disorganized, but actin patches were still present. Secondly, these patches were formed at a considerable distance from the apical dome. Thirdly, the SPK was not disorganized and time-lapse sequences revealed that it was the origin of waves of actin
705 filaments that under these mutant conditions became, conspicuously visible. The fact that *dip1*Δ cells are able to maintain polarity and to generate actin patches show that there must be a mechanism alternative to Dip1 that mediates the biogenesis of endocytic actin structures. We propose that this mechanism is provided by cortical actin filaments deriving from the SPK, which could act as seeds for Arp2/3 in *dip1*Δ cells.

710

The highly speculative model depicted in Figure 16 aims to account for these observations as follows: under normal circumstances, Dip1, located at the position of the endocytic collar, activates Arp2/3 to synthesize linear filaments [16] which in turn prime the synthesis of branched actin networks that power endocytic internalization. These tip-
715 proximal patches eventually give rise to filaments that are severed by cofilin to form worms that move away from the tip and that, in addition of serving as seeds for tip-distal patches, have the potential to redistribute G-actin across the whole length of the hyphal tip cell. In *dip1*Δ cells the apical dome and the subtending region are free of actin patches, but actin filaments deriving from the SPK-localized formin are very prominent, extending
720 deep into the cell. These filaments would be responsible of providing mother filaments for actin patches, which would be excluded from the tip and its environs because one or more factors decorating these filaments/cables would compete with factors which are essential for the biogenesis of endocytic actin. An obvious candidate is tropomyosin, which outcompetes fimbrin from formin-derived actin cables whereas fimbrin
725 outcompetes tropomyosin from Arp2/3-derived actin networks [75, 76]. Lastly, an important observation is that tropomyosin is strongly concentrated in the F-actin-containing SPK (Figure 1C). This actin network is synthesized by the SepA formin (Figure 14A), and does not contain Arp2/3-branched actin (Figure 11), the possible mechanism being that this complex is outcompeted by tropomyosin also in this locale.
730

Materials and Methods

Aspergillus techniques

Aspergillus strains were grown on standard culture media [77]. Cassettes to generate fluorescent proteins or null mutants were introduced into the appropriate strains by
735 transformation and homologous recombination [78] using *nku*Δ recipient strains [79]. All strains were tested by PCR using oligonucleotides flanking the cassettes to ensure correct cassette integration. The full list of strains with their genotypes is listed in Table S1.

Null mutant strains and fluorescent protein tagging

740 All deletion mutations used in this work, namely *arpC1*Δ, *vpr1*Δ, *fimA*Δ, *srv2*Δ, *dip1*Δ, *cofA*Δ, *capA*Δ [67] and *abpA*Δ [6], were constructed by transformation and gene replacement using casettess generated by fusion PCR with appropriate selection markers. *niiAp::SlaB*^{Sla2} is a conditional expression allele, in which SlaB^{Sla2} (also denoted

SlaB) is expressed under the control of the nitrate-inducible, ammonium-repressible
745 nitrite reductase promoter [24]. *fimA::Tn341* is a transposon insertion 341 pb downstream from the start codon of *fimA* [4]. *sepA1* is a termosensitive allele encoding a mutant formin carrying a Leu1639Ser substitution. This residue lies in the conserved FH2 domain [62].TpmA-tdT, Lifeact-GFP/tdT, actin chromobody-mCherry/TAgGFP, Tractin-GFP and *Aspergillus* actin-GFP were expresed under the control of *inuA*
750 promoter. These cassettes were integrated into the *inuA* locus [47]. ArpC1-GFP, SepA-3xGFP, Vpr1-GFP, Srv2-GFP, Dip1-GFP, CapA-GFP, Cof1-GFP, FimA-mCherry, FimA-GFP, AbpA^{Abp1}-GFP/mRFP, SlaB^{Sla2}-GFP, MyoE-3xGFP, MyoE-mCherry were C-terminally tagged endogenously. ChsB was N-terminally tagged endogenously[7]. All cassettes were generated by fusion PCR using the primers listed in Supplementary
755 Table S2.

Details of F-actin reporters driven by the *inuA* promoter

All reporter proteins/peptides were separated from the fluorescent protein moieties by a (Gly-Ala)5 linker. Lifeact transgenes contain the 17 N-terminal amino acids of Abp140 from *S. cerevisiae* (MGVADLIKKKFESISKEE) fused to GFP or tdT. Actin chromobody
760 transgenes were constructed using the commercial plasmid Actin-Chromobody® TagGFP2 (ChromoTek #ACG) as template for PCR amplification of the coding region of α-actin nanobody. This fragment was used to generate by fusion PCR the TagGFP or mCherry cassettes with appropriate selection markers.The tractin reporter is composed of residues 10-52 of the rat inositol 1,4,5-triphosphate 3-kinase A (ITPKA) protein [31].
765 The DNA fragment coding for this reporter was synthesized by GenScrip (https://www.genscript.com/) and translationally fused by its C-terminus to the GFP coding region. The GFP-actin transgene expressed under the control of the *inuA* promoter was integrated by gene replacement at the *inuA* locus (inulinase is required only if *Aspergillus* is cultured on inulin as the only carbon source). The strain generated
770 has a backup untagged copy of the actin gene. The TpmA-TdTomato cassette was integrated in the *wA* locus and expressed under its own promoter. The strain generated has a backup untagged copy of TpmA.

Western blots

775 For quantitation of Lifeact expression levels in cells cultured on different glucose and sucrose concentrations, the Lifeact-GFP strain was grown overnight at 30°C in minimal medium (MMA) containing the different carbon sources indicated on Figure 1B. Total

protein extraction has been described [80]. The following antibodies were used: Lifeact-GFP; Merck'#11814460001 monoclonal anti-GFP as primary antibody (1/5000) and
780 HRP-conjugated AffiniPure goat anti-mouse IgG (H + L) secondary antibodies (Jackson Immunoresearch #115-035-003, 1/5000). For tubulin, anti α-tubulin (Merck # T9026) monoclonal as primary antibody and HRP-conjugated AffiniPure goat anti-mouse IgG (H + L) as secondary antibodies (Jackson Immunoresearch #115-035-003, 1/5000).Reacting bands were detected with Clarity western ECL substrate (Biorad
785 Laboratories #1705061)

Fluorescence microscopy

Aspergillus strains were cultured “on stage” in Ibidi 8-well μ-slide uncoated chambers (Ibidi Cat#80821), using “watch minimal medium” (WMN)[23] with 0.1% glucose as carbon source when expression was driven by the endogenous promoter, or with a
790 mixture of 0.05% glucose and 0.025% sucrose (w/v in all cases) when expression of the reporter genes was driven by the *inuA* promoter. All wide-field imaging was carried out in Leica DMi6 or DMi8 inverted microscopes. The details of the software, hardware, image acquisition, analysis and presentation have been thoroughly described [61]. Deconvolution was carried out with Huygens software (Scientific Volume Imaging B.V.).
795 Benomyl was used at 5 micrograms/ml, and latrunculin B at 100 micromolar.

Quantitation of the half-life of actin patches

For movies acquired at 5 fps, images (exposure time, 200 ms) were streamed to the memory of the computer using Metamorph software. Chimeric reporters usually allowed the acquisition of 600-900 frames. When needed, exposure times were increased and
800 the number of images modified accordingly to cover similar total times. For proteins residing in patches for long times, as is the case of $SlaB^{Sla2}$, or for certain mutants resulting in long lifetimes of Lifeact-GFP in patches, exposure times were increased to 1 sec. Lifetimes of the different reporters were deduced usually from longitudinal kymographs, unless otherwise indicated in the Figures. Actin patches gave rise to
805 vertical lines whose length reflects the time of residence of the reporter. When needed, overlapping signals were confirmed by using x,y,t stacks as if they were x,y,z stacks, and visualized using Imaris software, which allows rotation of stacks, thereby facilitating resolution of closely adjacent traces. The length of the traces was estimated visually using appropriate tools of Metamorph and converted into timescales. The analysis and
810 graphical representation of data were carried out with GraphPad Prism software (v. 7.03).

Endocytic recycling assays

Endocytic recycling polarizes cargoes such as ChsB. Therefore, we took the distance to which the transmembrane protein ChsB diffuses away from the apex as an indirect measurement of the efficiency of endocytosis. This distance was calculated with a line drawn with the “regions measurement” menu of Metamorph from the apex to the most basal point to which GFP-ChsB reached.

Confocal imaging

We used a Leica TCS SP8 scanning microscope equipped with a “white light” laser enabling precise excitation wavelength selection. In typical z-stack acquisitions such as that shown on Figure 11 C, we used a 63x immersion oil objective, with x,y,z dimensions of 50, 50, 200 nm at 1 AU, laser settings at 483 nm for the GFP channel and 585 nm for the mCherry channel, and standard PMT detection. Raw images were digitalized at 16 bits and manipulated using LAS X software (Leica Microsystems GmbH).

Acknowledgements

We thank Brian Shaw, Xin Xiang and Berl Oakley for generously sharing strain and to Sara Abib for skillful technical assistance. This work has been supported by Grants TED2021-129607B-I00 funded by MCIN/AEI/ 10.13039/501100011033 and by the “European Union NextGeneration EU/PRTR”, and by Grant PID2021-124278OB-I00 funded by MCIN/AEI/ 10.13039/501100011033 and “ERDF A way of making Europe”, to EAE and MAP. MD was supported by a FPI Grant PRE2022-102144 funded by MCIN/AEI/ 10.13039/501100011033 and by “ESF Investing in your future”

Legends to Figures

Figure 1: A summary of the reporters used to detect F-actin structures

(A) Localization of TpmA-tdTomato (tdT). Top, ribbon scheme of TpmA-tdT. Bottom, left: The image is a deconvolved middle plane of a hyphal tip cell showing the localization of
840 TpmA-tdT to the SPK (asterisk). Bottom, right: consecutive planes of a Z-stack showing the SPK (asterisk) and the actin cables that emerge from it (Z= 0.5 um).
(B) Western blot analysis of Lifeact-GFP expression levels on different carbon sources. Tubulin was used as loading control.
(C) Expression of Lifeact-GFP does not cause defects in apical extension. Quantitation
845 of apical extension rates in the wild-type and in a Lifeact-GFP strain. Time stacks acquired with Nomarski optics at 28°C were used to calculate apical extension rates of individual cells with kymographs. Error bars indicate the mean ± S.D. Means were compared by Student's *t*-test; ns, non-significant.
(D) Localization of the different actin reporters. Top, schematics depicting the structures
850 of the different actin reporter constructs. Below, fluorescence images of the localization of the different actin reporters. Images are maximal intensity projections of deconvolved Z-stacks. The SPK, endocytic collar, actin filaments, and actin patches can be observed. All reporters additionally labeled septa, but only one example is shown for tagGFP.

855 **Figure 2. The actin cytoskeleton visualized with Lifeact**

(A) Relationship between actin and microtubule cytoskeletons. F-actin visualized with Lifeact-tdT and MTs with TubA-GFP. Images are MIPS of a deconvolved Z-stack.
(B) The density of actin patches in the endocytic collar is at least three times higher than in distal regions of the hypha. Lifeact-GFP image (middle plane) showing SPK, actin
860 patches and endocytic collar (shadowed yellow). Graph quantifying the signal intensity of Lifeact-GFP in the endocytic collar region and in distal regions of the hypha. Error bars show mean ± S.D.
(C) Graph representing the distance from the endocytic collar to the apex. Error bars show mean ± S.D. (*N*=12)
865 (D) Graph representing the perimeter of the apical dome. Error bars show mean ± S.D. (*N*=12)
(E) MIP of a time-lapse sequence of the F-actin cytoskeleton visualized with Lifeact-GFP that illustrates how the endocytic collar and the SPK advance coordinately.

(F) Three-dimensional reconstruction of a confocal z-stack showing the spatial
870 relationship between the endocytic collar and the SPK.
(G) Hyphal tip cell illustrating how the plus-end of MTs reach the SPK. Images are MIPs of a dual-channel Z-stack of F-actin labeled with Lifeact-tdT and MTs labeled with two TubA-GFP. The box on the right is a (z, y) orthogonal view of the region of the SPK, showing colocalization.
875 (H) The organization of the F-actin and MT cytoskeletons is mutually dependent. Hyphal tip cell treated with latrunculin B, which depolymerizes the F-actin cytoskeleton completely, but not the MTs, although the plus-ends of these no longer concentrate in the apex, and are instead spread across the apical dome, which is clearly swollen.
(I) Hyphal tip cell treated with benomyl, showing that while MTs are completely
880 depolymerized, F-actin is not, although the F-actin cytoskeleton is completely disorganized and the actin collar is no longer present.
(J) Different frames of a time-lapse sequence (supplemental movie 3) showing F-actin labeled with Lifeact-GFP and chromatin labeled with HhoA-mCh.

885 **Figure 3. Determining the behavior and lifetime of actin patches visualized with F-actin reporters.**

(A) Kymograph derived from a time-lapse sequence of Lifeact-GFP acquired with a time resolution of 2 fps. The indicated rectangular region is magnified on the right. Note the tilted line corresponding to the endocytic collar is moving ahead with tip growth,
890 demonstrating that imaging conditions do not impair growth.
(B) Kymograph derived from the time-lapse sequence of Lifeact-GFP made with images acquired every 0.2 seconds for 3 minutes. The indicated rectangular region is magnified on the right.
(C) Behavior of individual actin patches. Images obtained from longitudinal (top) or
895 transverse (bottom) kymographs.
(D) Half-life, in seconds, of actin patches labeled with the different reporters indicated in the graph. Error bars indicate mean +/- S.D. Values were obtained from individual patches extracted from kymographs with a time resolution of 5 fps.

900 **Figure 4. Actin patches associate with actin filaments**

(A) Actin patches are associated with cortical filaments. Consecutive planes of a z-stack of Lifeact -GFP (z=0. 25 μm). The graph is a linescan across the ROI indicated

(B) MIP of a z-stack of Lifeact -GFP.

(C) Still images extracted from supplemental movie 6 showing the formation of patches associated with filaments (arrows, each patch is color-coded). Numbering indicates time in seconds.

(D) Still images from a time-lapse acquisition at 2 fps showing an example of an actin filament (tail indicated by a blue arrowhead) nucleated from a patch (red arrowhead).

(E) Still images showing different aspects of the dynamics of actin filaments labeled with Lifeact-GFP. Numbers indicate time in seconds. The tip (not shown) is at the top. The pink-shaded filament grows during the first two minutes of the sequence before moving towards the base. The yellow-shaded filament is severed at the 36 seconds time-point. The blue-shaded portion appears to be depolymerized, whereas the yellow portion moves towards the base as it is being depolymerized

(F) Kymograph derived from a Lifeact-tdT time series acquired at 5 fps. Filaments moving away from the tip, occupied by a prominent actin collar, are seen as diagonal lines. The graphs represent the speed of this basipetal movements and the average length travelled by these filaments. Error bars indicate S. D.

(G) The time series that gave origin to this kymograph were acquired at 6 fpm (see supplemental movie 11). It illustrates the long distances that can be covered by moving filaments.

Figure 5. Localization and dynamics of AbpA^{Abp1} and SlaB^{Sla2}.

(A) Localization de AbpA^{Abp1}-mRFP (top) and AbpA^{Abp1}-GFP (bottom). Images are middle planes of deconvolved z-stacks.

(B) Time of residence of AbpA^{Abp1}-GFP in patches. Error bars represent S.D. The kymograph on the right has time resolution of 5 fps.

(C) Localization of endogenously tagged SlaB^{Sla2}-GFP. The image is a middle plane of a deconvolved z-stack illustrating the cortical localization of this protein.

(D) Time of residence of SlaB^{Sla2}-GFP in patches. Error bars represent S.D.

(E) Kymographs derived from a time-lapse sequence with simultaneous acquisition of Lifeact-tdT and SlaB^{Sla2}-GFP channels.

(F) Spores from a strain carrying a conditional SlaB^{Sla2} expression allele permitting expression on nitrate but not on ammonium were germinated on minimal medium containing ammonium as sole carbon source. The resulting germlings were able to establish polarity but not to maintain it, arresting growth with a characteristic “yeast-like”

morphology. In these germlings, Lifeact-GFP appears as clumps associated with the plasma membrane. The image is a middle plane of a deconvolved z-stack.

940 **Figure 6. Localization and dynamics of fimbrin-GFP**

(A) Localization of fimbrin-GFP. The image is a maximum intensity projection of deconvolved Z-stack, pseudo-colored in cyan to distinguish this reporter from images of Lifeact-GFP also included in the Figure.

(B) Time of residence of FimA-GFP patches. Error bars represent mean +/- S.D. The
945 kymograph was extracted from a movie acquired at 5 fps.

(C) Localization of Lifeact-GFP in wild-type and *fimA::Tn341* hyphal tip cells. Images are MIPs of deconvolved Z-stacks.

(D) Growth test of indicated strains on complete medium at 37ºC.

(E) Terminal phenotype of a *fimA*Δ germling expressing Lifeact-GFP. Spores from a
950 *fimA*+/ *fimA*Δ heterokaryon were inoculated on selective medium, in which only the *fimA*Δ haploid spores germinate. The image is a MIP of a deconvolved Z-stack.

(F) Dynamics of actin patches in *fimA::Tn341*. Grayscale longitudinal kymographs comparing the behavior of Lifeact -GFP actin patches in the mutant with the wild type. F-actin stays in the patches for a longer period in *fimA::Tn341* (see also Figure 7) and the
955 mutant patches are static. The colored traces shown below correspond to transverse kymographs. Examples depicting individual frames of wild type and *fimA::Tn341* time series are shown on the right.

Figure 7. Lifeact-GFP patches in mutant backgrounds.

960 Error bars indicate the mean +/- S.D. Data sets were compared to the wild-type by ANOVA using Dunnet's multiple comparisons test.

Figure 8. Cofilin is essential.

(A) Heterokaryon rescue test. Haploid conidiospores obtained from heterokaryotic
965 mycelia carrying *cof1+ pyrG89* and *pyrG89 cof1*Δ*::pyrG+* nuclei were streaked on medium without pyrimidines, which selected against the wild type. Haploid *pyrG89 cof1*Δ::*pyrG*$^{+}$ streaks did not give rise to visible growth, whereas a heterozygous diploid

used as a control grew normally. Note that spores acquire a single nucleus during conidiogenesis, thereby resolving heterokaryosis.

970 (B) Terminal phenotype with which *cof1*Δ germlings arrest growth, after 18 hours of incubation at 25°C. Yellow asterisks indicate *pyrG89 cof1*Δ::*pyrG*$^+$ germlings with the characteristic yeast-like phenotype, whereas cyan asterisks indicate *pyrG89 cof1*$^+$ conidia unable to establish polarity.

(C) Localization of Lifeact-GFP in *cof1*Δ mutant germling. The image is a middle plane

975 of a deconvolved Z-stack.

(D) Localization of endogenously tagged Cof1-GFP in heterozygosis with a wild-type allele in a diploid strain. Note the presence of cofilin in the actin collar. The image is an MIP of a deconvolved z-stack.

980 **Figure 9. The role of Srv2/CAP in endocytosis.**

(A) Growth tests showing that *srv2Δ* markedly impairs colony growth, with the endogenously GFP-tagged allele resulting in an intermediate growth phenotype, indicative of partial-loss-of-function

(B) Lifeact-GFP imaging shows that *srv2Δ* disrupts the normal distribution of actin

985 patches and delocalizes actin from the SPK. Images are MIPs of deconvolved Z-stacks. The boxed region is a middle plane showing the disorganization of the endocytic collar.

(C) Kymograph analysis of wild-type and *srv2Δ* time-lapse sequences of Lifeact-GFP acquired at 5 fps. The *srv2Δ* lifetime of actin patches is depicted on Figure 7

(D) Endocytic recycling of GFP-ChsB: in the wild-type, this cargo of the endocytic

990 recycling pathway is polarized by endocytosis to the approximately 2 µm region from the apex, mostly corresponding to the apical dome. In contrast, in *srv2Δ* hyphae, GFP-ChsB is spread regions several microns away from the apex due to the endocytic deficit of the mutant. Error bars, mean +/- S.D.

(E) This F-actin worm appears to consist of 2 parallel filaments seemingly propelled by

995 forces originating at the tail. The box on the right shows the corresponding longitudinal kymograph indicating that these filaments move at an average speed of 0.35 µm/s.

Figure 10. The Arp2/3 complex arrives at actin patches at roughly the same time than F-actin.

1000 (A) *arpC1Δ* ablating a key subunit of the Arp2/3 complex results in lethality. The Nomarski image shows that *arpC1Δ* spores, collected from heterokaryotic mycelia, give rise to germlings that arrested growth shortly after establishing polarity, with the typical morphology of cells deficient in endocytosis.

(B) Growth tests showing that endogenously tagged ArpC1 (*arpC1-GFP*) is functional

1005 (C) ArpC1-GFP localizes to actin patches

(D) Kymograph analysis: ArpC1-GFP resides in actin patches for approximately 14 sec.

(E) ArpC1-GFP and F-actin (Lifeact-tdT) colocalize across time.

(F) Analysis of the relative signals of ArpC1-GFP and Lifeact-tdT in N = 5 patches. Each frame corresponds to 200 msec of a time-lapse series with simultaneous acquisition of

1010 the two channels using a Gemini beam splitter.

Figure 11. The Arp2/3 complex is excluded from the SPK

(A) MIPs showing the localization of MyoE-GFP to the apex, whereas secretory vesicles labeled with FM4-64 display a slightly broader distribution at the tip.

1015 (B) Left, composite confocal image showing the localization of the SepA formin to the apex. Right, SepA and MyoE colocalize at the SPK.

(C) Arp2/3, labeled with ArpC1-GFP, is absent from the SPK, labeled with MyoE-mCh. Images are MIP of a confocal z-stack.

1020 **Figure 12. The motile phase of actin patches is dependent on Vpr1.**

(A) Marked growth defects of *vpr1Δ cells*.

(B) Endogenously tagged Vpr1-GFP is functional and localizes to actin patches. Consecutive sections of a z-stack and MIP (colored, heat LUT).

(C) Kymographs comparing the behavior of Vpr1-GFP with ArpC1-GFP, derived from

1025 time lapse acquisitions at 5 fps. The lifetime of Vpr1-GFP is approximately half that of ArpC1-GFP.

(D) The presence of Vpr1 on actin patches is restricted to the first half of the actin module.

(E) and (F) Kymographs showing that the lifetime of Lifeact-GFP in *vpr1Δ* cells doubles that of the wild-type (see also Figure 7), and that *vpr1Δ* patches lack the motile phase.

1030 (G) Z-series and MIPs of GFP-ChsB in *vpr1Δ* compared to the wild-type show the markedly longer distance to which ChsB diffuses across the membrane, indicative of a major defect in endocytic recycling.

Figure 13. Synthetic negative interaction of *abpAΔ* and *capAΔ* mutants

1035 (A) AbpA^{Abp1}-mRFP localizes to the endocytic collar but not to the SPK, labelled with SepA. The image is a MIP. The asterisk indicates the SPK.

(B) Top: Growth tests showing that *abpAΔ*, which by itself does not cause any noticeable defect, shows a strong synthetic negative interaction with *capAΔ*. Bottom: Progeny of a heterozygous cross between *abpA*Δ and *capA*Δ parental strains spread on a plate,
1040 highlighting the severe growth impairment in the *abpAΔ capA*Δ double mutant.

(C) Maximum intensity projections (MIP) of Lifeact-GFP showing that *capAΔ* but not *abpAΔ* delocalizes actin from the SPK (arrowheads).

(D) CapA-GFP (golden LUT) localizes to the SPK (indicated with an asterisk), whereas AbpA^{Abp1}-GFP (yellow LUT) does not.

1045 (E) Diffusion across the plasma membrane of GFP-ChsB is normal in the single *abpAΔ* mutant, significantly increased in the single *capAΔ* mutant and markedly elevated in the double mutant, indicating progressively increasing endocytic deficit.

Figure 14. Conditional inactivation of formin does not affect the lifecycle
1050 **of actin in patches**

(A) Delocalization of F-actin from the SPK (indicated with an asterisk) in cells carrying the *sepA1 ts* mutation at the restrictive (37ºC), but not at the permissive (30ºC) temperature.

(B) Kymographs (5 fps) of Lifeact-GFP at the indicated temperatures and mutant
1055 conditions analysis. Graphs on the right show the corresponding quantitative analyses of time of residence. Box and whiskers error bars are minimal to maximum; datasets were analyzed by ANOVA followed by Tukey's multiple comparison test; n.s., non-significant; ****, $P < 0.001$.

(C) As above, but using FimA-mCh as reporter.

1060

Figure 15. Dip1 is a key regulator of endocytic F-actin.

(A) Localization of Dip1-GFP to the endocytic collar. MIP of a deconvolved Z-stack

(B) *dip1Δ* results in a marked growth defect.

(C) *dip1Δ* does not delocalize SepA from the SPK. Middle plane of a deconvolved Z-
1065 stack.

(D) Prominent acting cables originating at the SPK become visible in the *dip1*Δ mutant.

(E) The actin collar is disorganized and actin patches appeared to be excluded from the region occupied by actin cables including the apical dome and subtending regions

(F) Kymographs of Lifeact-GFP capture how actin filaments originate regularly at the
1070 region of the SPK, diagonal lines.

(G) Analysis of Lifeact-GFP actin patches in *dip1Δ* cells (time resolution is 5 fps).

(H) The Endocytic collar is disorganized in *dip1Δ* cells, using fimbrin-GFP as reporter.

(I) The Lifetime of fimbrin-GFP In *dip1Δ* cells closely resembles that of Lifeact.

(J) Example of an actin filament elongating throughout the sequence of 53 seconds (its
1075 leading end is indicated with a red dot). Some actin patches appeared to develop associated with the filament, whereas other appear to be captured by the growing end.

(K) Endocytic recycling of ChsB is markedly affected, such that the reporter diffuses away from the tip for notable distances. The color images are maximal intensity projections represented with a heat LUT.

1080 **Figure 16. A model for the biogenesis of actin patches**

See text for details. In the absence of Dip1, filaments originating from the severing of actin cables synthesized by SPK-localized formin serve as seeds for the Arp2/3 actin branching complex.

1085

References

1. Jahn R, Fasshauer D. Molecular machines governing exocytosis of synaptic vesicles. Nature. 2012;490(7419):201-7. doi: 10.1038/nature11320.

2. Gundelfinger ED, Fejtova A. Molecular organization and plasticity of the
1090 cytomatrix at the active zone. Current Opinion in Neurobiology. 2012;22(3):423-30. doi: https://doi.org/10.1016/j.conb.2011.10.005.

3. Siksou L, Triller A, Marty S. Ultrastructural organization of presynaptic terminals. Current Opinion in Neurobiology. 2011;21(2):261-8. doi: https://doi.org/10.1016/j.conb.2010.12.003.

1095 4. Upadhyay S, Shaw BD. The role of actin, fimbrin and endocytosis in growth of hyphae of *Aspergillus nidulans.* Molecular Microbiology. 2008;3:690-705. doi: 10.1111/j.1365-2958.2008.06178.x.

5. Taheri-Talesh N, Horio T, Araujo-Bazan L, Dou X, Espeso EA, Penalva MA, et al. The tip growth apparatus of *Aspergillus nidulans*. Molecular Biology of the Cell.
1100 2008;19(4):1439-49. doi: 10.1091/mbc.E07-05-0464. PubMed PMID: WOS:000258951500015.

6. Araujo-Bazán L, Peñalva MA, Espeso EA. Preferential localization of the endocytic internalization machinery to hyphal tips underlies polarization of the actin cytoskeleton in Aspergillus nidulans. Mol Microbiol. 2008;67(4):891-905. Epub
1105 20080107. doi: 10.1111/j.1365-2958.2007.06102.x. PubMed PMID: 18179595.

7. Hernández-González M, Bravo-Plaza I, Pinar M, de los Rios V, Arst HN, Jr., Peñalva MA. Endocytic recycling via the TGN underlies the polarized hyphal mode of life. Plos Genetics. 2018;14(4):e1007291. doi: 10.1371/journal.pgen.1007291. PubMed PMID: WOS:000431115700013.

1110 8. Peñalva MA, Galindo A, Abenza JF, Pinar M, Calcagno-Pizarelli AM, Arst HN, et al. Searching for gold beyond mitosis: Mining intracellular membrane traffic in Aspergillus nidulans. Cell Logist. 2012;2(1):2-14. doi: 10.4161/cl.19304. PubMed PMID: 22645705; PubMed Central PMCID: PMCPMC3355971.

9. Abenza JF, Pantazopoulou A, Rodriguez JM, Galindo A, Penalva MA. Long-
1115 Distance Movement of Aspergillus nidulans Early Endosomes on Microtubule Tracks. Traffic. 2009;10(1):57-75. doi: 10.1111/j.1600-0854.2008.00848.x. PubMed PMID: WOS:000262131600006.

10. Pantazopoulou A, Peñalva MA. Characterization of *Aspergillus nidulans* RabC/Rab6. Traffic. 2011;12(4):386-406. doi: 10.1111/j.1600-0854.2011.01164.x.
1120 PubMed PMID: WOS:000288546900004.

11. Weinberg J, Drubin DG. Clathrin-mediated endocytosis in budding yeast. Trends Cell Biol. 2012;22(1):1-13. Epub 20111020. doi: 10.1016/j.tcb.2011.09.001. PubMed PMID: 22018597; PubMed Central PMCID: PMCPMC3253927.

12. Kaksonen M, Toret CP, Drubin DG. A modular design for the clathrin- and actin-mediated endocytosis machinery. Cell. 2005;123(2):305-20. doi: 10.1016/j.cell.2005.09.024.

13. Kaksonen M, Sun Y, Drubin DG. A pathway for association of receptors, adaptors, and actin during endocytic internalization. Cell. 2003;115:475-87.

14. Kaksonen M, Roux A. Mechanisms of clathrin-mediated endocytosis. Nat Rev Mol Cell Biol. 2018;19(5):313-26. Epub 2018/02/08. doi: 10.1038/nrm.2017.132.

15. Basu R, Chang F. Characterization of dip1p reveals a switch in Arp2/3-dependent actin assembly for fission yeast endocytosis. Current Biology. 2011;21(11):905-16. doi: 10.1016/j.cub.2011.04.047.

16. Balzer CJ, Wagner AR, Helgeson LA, Nolen BJ. Dip1 Co-opts Features of Branching Nucleation to Create Linear Actin Filaments that Activate WASP-Bound Arp2/3 Complex. Curr Biol. 2018;28(23):3886-91.e4. Epub 20181121. doi: 10.1016/j.cub.2018.10.045. PubMed PMID: 30471998; PubMed Central PMCID: PMCPMC6292448.

17. Wagner AR, Luan Q, Liu SL, Nolen BJ. Dip1 defines a class of Arp2/3 complex activators that function without preformed actin filaments. Curr Biol. 2013;23(20):1990-8. Epub 20131010. doi: 10.1016/j.cub.2013.08.029. PubMed PMID: 24120641; PubMed Central PMCID: PMCPMC3930447.

18. Zou S, Chen Y, Liu Y, Segev N, Yu S, Min G, et al. Trs130 participates in autophagy through GTPases Ypt31/32 in Saccharomyces cerevisiae. Traffic. 2013;14(2):233-46. doi: 10.1111/tra.12024.

19. Echauri-Espinosa RO, Callejas-Negrete OA, Roberson RW, Bartnicki-García S, Mouriño-Pérez RR. Coronin is a component of the endocytic collar of hyphae of Neurospora crassa and is necessary for normal growth and morphogenesis. PLoS ONE. 2012;7(5):e38237. Epub 2012/06/14. doi: 10.1371/journal.pone.0038237 PONE-D-12-03973 [pii].

20. Bartnicki-Garcia S, Garduno-Rosales M, Delgado-Alvarez DL, Mourino-Perez RR. Experimental measurement of endocytosis in fungal hyphae. Fungal Genet Biol. 2018;118:32-6. Epub 2018/07/19. doi: 10.1016/j.fgb.2018.07.001.

21. Lara-Rojas F, Bartnicki-García S, Mouriño-Pérez RR. Localization and role of MYO-1, an endocytic protein in hyphae of Neurospora crassa. Fungal Genetics and Biology. 2016;88:24-34. doi: 10.1016/j.fgb.2016.01.009.

22. Delgado-Álvarez DL, Callejas-Negrete OA, Gómez N, Freitag M, Roberson RW, Smith LG, et al. Visualization of F-actin localization and dynamics with live cell markers in Neurospora crassa. Fungal Genetics and Biology. 2010;47(7):573-86. doi: 10.1016/j.fgb.2010.03.004.

23. Peñalva MA. Tracing the endocytic pathway of Aspergillus nidulans with FM4-64. Fungal Genetics and Biology. 2005;42(12):963-75
doi: 10.1016/j.fgb.2005.09.004.

24. Hervás-Aguilar A, Peñalva MA. Endocytic machinery protein SlaB is dispensable for polarity establishment but necessary for polarity maintenance in hyphal tip cells of

Aspergillus nidulans. Eukaryotic Cell. 2010;9(10):ec.00119-10. doi: 10.1128/EC.00119-10.

25. Peñalva MA. Endocytosis in filamentous fungi: Cinderella gets her reward. Current Opinion in Microbiology. 2010;13(6):084-692
1170 doi: 10.1016/j.mib.2010.09.005.

26. Vasselli JG, Kainer E, Shaw BD. Using fimbrin to quantify the endocytic subapical collar during polarized growth in three filamentous fungi. Mycologia. 2023;115(4):456-69. Epub 20230517. doi: 10.1080/00275514.2023.2202689. PubMed PMID: 37196171.

27. Berepiki A, Lichius A, Shoji JY, Tilsner J, Read ND. F-actin dynamics in
1175 Neurospora crassa. Eukaryotic Cell. 2010;9(4):547-57. doi: 10.1128/EC.00253-09.

28. Schultzhaus Z, Quintanilla L, Hilton A, Shaw BD. Live Cell Imaging of Actin Dynamics in the Filamentous Fungus Aspergillus nidulans. Microsc Microanal. 2016;22(2):264-74. Epub 20160216. doi: 10.1017/S1431927616000131. PubMed PMID: 26879694.

1180 29. Li YB, Xu R, Liu C, Shen N, Han LB, Tang D. Magnaporthe oryzae fimbrin organizes actin networks in the hyphal tip during polar growth and pathogenesis. PLoS Pathogens. 2020;16(3):e1008437. doi: 10.1371/journal.ppat.1008437.

30. Melak M, Plessner M, Grosse R. Actin visualization at a glance. J Cell Sci. 2017;130(3):525-30. Epub 2017/01/14. doi: 10.1242/jcs.189068.

1185 31. Belin BJ, Goins LM, Mullins RD. Comparative analysis of tools for live cell imaging of actin network architecture. BioArchitecture. 2014;4(6):189-202. doi: 10.1080/19490992.2014.1047714.

32. Riquelme M, Sánchez-León E. The Spitzenkörper: a choreographer of fungal growth and morphogenesis. Current Opinion in Microbiology. 2014;20:27-33. doi:
1190 10.1016/j.mib.2014.04.003.

33. Bartnicki-García S, Bartnicki DD, Gierz G, López-Franco R, Bracker CE. Evidence that Spitzenkörper behavior determines the shape of a fungal hypha: a test of the hyphoid model. Exp Mycol. 1995;19(2):153-9. doi: 10.1006/emyc.1995.1017.

34. Pantazopoulou A, Pinar M, Xiang X, Peñalva MA. Maturation of late Golgi
1195 cisternae into RabE(RAB11) exocytic post-Golgi carriers visualized in vivo. Molecular Biology of the Cell. 2014;25(16):2428-43. doi: 10.1091/mbc.E14-02-0710. PubMed PMID: WOS:000340997100011.

35. Peñalva MA, Zhang J, Xiang X, Pantazopoulou A. Transport of fungal RAB11 secretory vesicles involves myosin-5, dynein/dynactin/p25 and kinesin-1 and is
1200 independent of kinesin-3. Molecular Biology of the Cell. 2017;28(1):947-61. doi: 10.1091/mbc.E16-08-0566.

36. Pinar M, Alonso A, de los Ríos V, Bravo-Plaza I, de la Gándara Á, Galindo A, et al. The type V myosin-containing complex HUM is a RAB11 effector powering movement of secretory vesicles. iScience. 2022;25(7):104514
1205 doi: 10.1016/j.isci.2022.104514.

37. Pinar M, Arst HN, Jr., Pantazopoulou A, Tagua VG, De Los Ríos V, Rodríguez-Salarichs J, et al. TRAPPII regulates exocytic Golgi exit by mediating nucleotide

exchange on the Ypt31 ortholog RabE^{RAB11}. Proc Natl Acad Sci USA. 2015;112(14):4346-51. doi: 10.1073/pnas.1419168112.

38. Harispe L, Portela C, Scazzocchio C, Penalva MA, Gorfinkiel L. Ras GTPase-activating protein regulation of actin cytoskeleton and hyphal polarity in Aspergillus nidulans. Eukaryotic Cell. 2008;7(1):141-53. doi: 10.1128/EC.00346-07. PubMed PMID: WOS:000258620200013.

39. Pearson CL, Xu K, Sharpless KE, Harris SD. MesA, a novel fungal protein required for the stabilization of polarity axes in Aspergillus nidulans. Molecular Biology of the Cell. 2004;15(8):3658-72. doi: 10.1091/mbc.E03-11-0803.

40. Hodges AR, Krementsova EB, Bookwalter CS, Fagnant PM, Sladewski TE, Trybus KM. Tropomyosin is essential for processive movement of a class V myosin from budding yeast. Current Biology. 2012;22(15):1410-6. Epub 2012/06/19. doi: 10.1016/j.cub.2012.05.035 S0960-9822(12)00588-X [pii].

41. Clayton JE, Pollard LW, Sckolnick M, Bookwalter CS, Hodges AR, Trybus KM, et al. Fission yeast tropomyosin specifies directed transport of myosin-V along actin cables. Mol Biol Cell. 2014;25(1):66-75. Epub 2013/11/08. doi: 10.1091/mbc.E13-04-0200.

42. Pruyne DW, Schott DH, Bretscher A. Tropomyosin-containing actin cables direct the Myo2p-dependent polarized delivery of secretory vesicles in budding yeast. Journal of Cell Biology. 1998;143(7):1931-45. Epub 1998/12/29.

43. Osmani SA, Engle DB, Doonan JH, Morris NR. Spindle formation and chromatin condensation in cells blocked in interphase by mutation of a negative cell cycle control gene. Cell. 1988;52:241-51. doi: 10.1016/0092-8674(88)90513-2.

44. Bergs A, Ishitsuka Y, Evangelinos M, Nienhaus GU, Takeshita N. Dynamics of Actin Cables in Polarized Growth of the Filamentous Fungus Aspergillus nidulans. Front Microbiol. 2016;7:682-. Epub 2016/06/01. doi: 10.3389/fmicb.2016.00682.

45. Hatano T, Lim TC, Billault-Chaumartin I, Dhar A, Gu Y, Massam-Wu T, et al. mNG-tagged fusion proteins and nanobodies to visualize tropomyosins in yeast and mammalian cells. Journal of Cell Science. 2022;135(18). doi: 10.1242/JCS.260288/VIDEO-15.

46. Belyy A, Merino F, Sitsel O, Raunser S. Structure of the Lifeact–F-actin complex. PLOS Biology. 2020;18(11):e3000925. doi: 10.1371/JOURNAL.PBIO.3000925.

47. Hernández-González M, Pantazopoulou A, Spanoudakis D, Seegers CLC, Peñalva MA. Genetic dissection of the secretory route followed by a fungal extracellular glycosyl hydrolase. Molecular Microbiology. 2018;109(6):781-800. doi: doi:10.1111/mmi.14073.

48. Bravo-Plaza I, Tagua VG, Arst HN, Alonso A, Pinar M, Monterroso B, et al. The Uso1 globular head interacts with SNAREs to maintain viability even in the absence of the coiled-coil domain. eLife. 2023;12:e85079. doi: 10.7554/eLife.85079.

49. Horio T, Oakley BR. The role of microtubules in rapid hyphal tip growth of Aspergillus nidulans. Molecular Biology of the Cell. 2005;16(2):918-26. doi: 10.1091/mbc.E04-09-0798.

50. Lizarrondo J, Klebl DP, Niebling S, Abella M, Schroer MA, Mertens HDT, et al. Structure of the endocytic adaptor complex reveals the basis for efficient membrane

anchoring during clathrin-mediated endocytosis. Nature Communications. 2021;12(1):2889. doi: 10.1038/s41467-021-23151-7.

51. Skruzny M, Brach T, Ciuffa R, Rybina S, Wachsmuth M, Kaksonen M. Molecular basis for coupling the plasma membrane to the actin cytoskeleton during clathrin-mediated endocytosis. Proc Natl Acad Sci U S A. 2012;109(38):E2533-42. Epub 20120827. doi: 10.1073/pnas.1207011109. PubMed PMID: 22927393; PubMed Central PMCID: PMCPMC3458359.

52. Young ME, Cooper JA, Bridgman PC. Yeast actin patches are networks of branched actin filaments. Journal of Cell Biology. 2004;166(5):629-35. doi: 10.1083/JCB.200404159.

53. Goode BL, Eskin J, Shekhar S. Mechanisms of actin disassembly and turnover. J Cell Biol. 2023;222(12). Epub 20231110. doi: 10.1083/jcb.202309021. PubMed PMID: 37948068; PubMed Central PMCID: PMCPMC10638096.

54. Lappalainen P, Drubin DG. Cofilin promotes rapid actin filament turnover *in vivo*. Nature. 1997;388(6637):78-82. doi: 10.1038/40418. PubMed PMID: 9214506.

55. Kotila T, Wioland H, Enkavi G, Kogan K, Vattulainen I, Jégou A, et al. Mechanism of synergistic actin filament pointed end depolymerization by cyclase-associated protein and cofilin. Nat Commun. 2019;10(1):5320. Epub 20191122. doi: 10.1038/s41467-019-13213-2. PubMed PMID: 31757941; PubMed Central PMCID: PMCPMC6876575.

56. Johnston AB, Collins A, Goode BL. High-speed depolymerization at actin filament ends jointly catalysed by Twinfilin and Srv2/CAP. Nature Cell Biology 2015 17:11. 2015;17(11):1504-11. doi: 10.1038/ncb3252.

57. Lewis MJ, Nichols BJ, Prescianotto-Baschong C, Riezman H, Pelham HR. Specific retrieval of the exocytic SNARE Snc1p from early yeast endosomes. Molecular Biology of the Cell. 2000;11:23-38. doi: 10.1091/mbc.11.1.23.

58. Goley ED, Welch MD. The ARP2/3 complex: An actin nucleator comes of age. Nature Reviews Molecular Cell Biology. 2006;7:713-26. doi: 10.1038/nrm2026.

59. Taheri-Talesh N, Xiong Y, Oakley BR. The Functions of Myosin II and Myosin V Homologs in Tip Growth and Septation in *Aspergillus nidulans*. PLoS One. 2012;7(2):e31218. doi: 10.1371/journal.pone.0031218.

60. Fischer-Parton S, Parton RM, Hickey PC, Dijksterhuis J, Atkinson HA, Read ND. Confocal microscopy of FM4-64 as a tool for analysing endocytosis and vesicle trafficking in living fungal hyphae. Journal of Microscopy. 2000;198:246-59. doi: 10.1046/j.1365-2818.2000.00708.x.

61. Pinar M, Peñalva MA. *En bloc* TGN recruitment of *Aspergillus* TRAPPII reveals TRAPP maturation as unlikely to drive RAB1-to-RAB11 transition. J Cell Sci. 2020;133(10):jcs241141. Epub 20200527. doi: 10.1242/jcs.241141. PubMed PMID: 32327558.

62. Sharpless KE, Harris SD. Functional characterization and localization of the Aspergillus nidulans formin SEPA. Mol Biol Cell. 2002;13(2):469-79. doi: 10.1091/mbc.01-07-0356. PubMed PMID: 11854405; PubMed Central PMCID: PMCPMC65642.

63. MacQuarrie CD, Mangione MSC, Carroll R, James M, Gould KL, Sirotkin V. The S. pombe adaptor protein Bbc1 regulates localization of Wsp1 and Vrp1 during endocytic actin patch assembly. Journal of Cell Science. 2019;132(17):jcs233502 doi: 10.1242/jcs.233502.

64. Aspenström P. The verprolin family of proteins: Regulators of cell morphogenesis and endocytosis. FEBS Letters2005. p. 5253-9.

65. Naqvi SN, Zahn R, Mitchell DA, Stevenson BJ, Munn AL. The WASp homologue Las17p functions with the WIP homologue End5p/verprolin and is essential for endocytosis in yeast. Current Biology. 1998;8(17):959-62 doi: 10.1016/s0960-9822(98)70396-3.

66. Sirotkin V, Beltzner CC, Marchand JB, Pollard TD. Interactions of WASp, myosin-I, and verprolin with Arp2/3 complex during actin patch assembly in fission yeast. J Cell Biol. 2005;170(4):637-48. Epub 20050808. doi: 10.1083/jcb.200502053. PubMed PMID: 16087707; PubMed Central PMCID: PMCPMC2171502.

67. Zhang J, Qiu R, Xiang X. The actin capping protein in Aspergillus nidulans enhances dynein function without significantly affecting Arp1 filament assembly. Sci Rep. 2018;8(1):11419. Epub 2018/08/01. doi: 10.1038/s41598-018-29818-4.

68. Michelot A, Grassart A, Okreglak V, Costanzo M, Boone C, Drubin DG. Actin Filament Elongation in Arp2/3-Derived Networks Is Controlled by Three Distinct Mechanisms. Developmental Cell. 2013;24(2):182-95. doi: 10.1016/j.devcel.2012.12.008.

69. Takeshita N, Mania D, Herrero S, Ishitsuka Y, Nienhaus GU, Podolski M, et al. The cell-end marker TeaA and the microtubule polymerase AlpA contribute to microtubule guidance at the hyphal tip cortex of *Aspergillus* nidulans to provide polarity maintenance. J Cell Sci. 2013;126(Pt 23):5400-11. Epub 20131007. doi: 10.1242/jcs.129841. PubMed PMID: 24101725.

70. Takeshita N, Higashitsuji Y, Konzack S, Fischer R. Apical sterol-rich membranes are essential for localizing cell end markers that determine growth directionality in the filamentous fungus *Aspergillus nidulans*. Mol Biol Cell. 2008;19(1):339-51. Epub 20071114. doi: 10.1091/mbc.e07-06-0523. PubMed PMID: 18003978; PubMed Central PMCID: PMCPMC2174190.

71. Balzer CJ, Wagner AR, Helgeson LA, Nolen BJ. Single-Turnover Activation of Arp2/3 Complex by Dip1 May Balance Nucleation of Linear versus Branched Actin Filaments. Curr Biol. 2019;29(19):3331-8.e7. Epub 20190926. doi: 10.1016/j.cub.2019.08.023. PubMed PMID: 31564494; PubMed Central PMCID: PMCPMC6783375.

72. Balzer CJ, James ML, Narvaez-Ortiz HY, Helgeson LA, Sirotkin V, Nolen BJ. Synergy between Wsp1 and Dip1 may initiate assembly of endocytic actin networks. Elife. 2020;9:e60419. Epub 20201112. doi: 10.7554/eLife.60419. PubMed PMID: 33179595; PubMed Central PMCID: PMCPMC7707826.

73. Burke TA, Christensen JR, Barone E, Suarez C, Sirotkin V, Kovar DR. Homeostatic actin cytoskeleton networks are regulated by assembly factor competition for monomers. Curr Biol. 2014;24(5):579-85. doi: 10.1016/j.cub.2014.01.072.

74. Chen Q, Pollard TD. Actin filament severing by cofilin dismantles actin patches and produces mother filaments for new patches. Curr Biol. 2013;23(13):1154-62. Epub 20130530. doi: 10.1016/j.cub.2013.05.005. PubMed PMID: 23727096; PubMed Central PMCID: PMCPMC4131202.

75. Christensen JR, Homa KE, Morganthaler AN, Brown RR, Suarez C, Harker AJ, et al. Cooperation between tropomyosin and a-actinin inhibits fimbrin association with actin filament networks in fission yeast. eLife. 2019;8:47279. doi: 10.7554/eLife.47279.001.

76. Homa KE, Hocky GM, Suarez C, Kovar DR. Arp2/3 complex- and formin-mediated actin cytoskeleton networks facilitate actin binding protein sorting in fission yeast. European Journal of Cell Biology. 2024;103(2):151404-. doi: 10.1016/J.EJCB.2024.151404.

77. Cove DJ. The induction and repression of nitrate reductase in the fungus Aspergillus nidulans. Biochim Biophys Acta. 1966;113(1):51-6. doi: 10.1016/s0926-6593(66)80120-0. PubMed PMID: 5940632.

78. Tilburn J, Scazzocchio C, Taylor GG, Zabicky-Zissman JH, Lockington RA, Davies RW. Transformation by integration in Aspergillus nidulans. Gene. 1983;26(2-3):205-21. doi: 10.1016/0378-1119(83)90191-9. PubMed PMID: 6368319.

79. Nayak T, Szewczyk E, Oakley CE, Osmani A, Ukil L, Murray SL, et al. A versatile and efficient gene-targeting system for Aspergillus nidulans. Genetics. 2006;172(3):1557-66. Epub 20051230. doi: 10.1534/genetics.105.052563. PubMed PMID: 16387870; PubMed Central PMCID: PMCPMC1456264.

80. Pinar M, Arias-Palomo E, de los Ríos V, Arst Jr HN, Peñalva MA. Characterization of Aspergillus nidulans TRAPPs uncovers unprecedented similarities between fungi and metazoans and reveals the modular assembly of TRAPPII. PLoS Genetics. 2019;15(12):e1008557. doi: 10.1371/journal.pgen.1008557.

Supporting information captions

1365 **The actin module of endocytic internalization in *Aspergillus nidulans*: a critical role of the WISH/DIP/SPIN90 family protein Dip1**

Marisa Delgado, Mario Pinar, Paula Polonio, Sergio Fandiño, Eduardo A. Espeso and Miguel A. Peñalva[1,*]

1370

Supplemental Figure 1

Lifetime of Cof1-GFP in a strain containing a wild-type copy of the *cof1* gene to rescue viability, as endogenous tagging of Cof1 is lethal.

1375 **Supplemental Figure 2**

(A) Ablation of Srv2 results in disorganization of the actin collar. (B) Localization of endogenously tagged Srv2-GFP. Note that the protein is not fully functional. Lifetime in actin patches of endogenously tagged Srv2-GFP and comparison with Lifeact-GFP patches in the wild-type. (D) "Worms" of F-actin moving towards the base of an *srv2Δ*
1380 strain, with a kymograph showing the corresponding speed.

Supplemental Figure 3

(A) Growth tests comparing the wild-type with a strain expressing endogenously tagged CapA-GFP and the corresponding *capAΔ* deletion mutant, showing that CapA-GFP is
1385 only partially functional. (B) Average lifetime of CapA-GFP in cortical patches. (C) Split tip in a *capA*Δ strain expressing Lifeact-GFP. (D) Multiple polarity axes in an *abpA*Δ *capA*Δ double mutant cell expressing Lifeact-GFP.

Supplemental Figure 4

1390 *sepA1* prevents growth at 37°C.

Supplemental Figure 5

(A) Growth test showing that Dip1-GFP is functional. (B) The apical extension rate of *dip1Δ* tips is half of the wild-type. (C) Deconvolved middle plane of a *dip1*Δ hypha
1395 expressing Lifeact-GFP. (D) Individual frames of a time-stack of a *dip1Δ* tip in which actin filaments emerge from the SPK.

Movies

1400 Supplemental movie 1: Overall view of the distribution of actin structures labeled with Lifeact-GFP over a period of one hour. Time is in min:sec:msec

Supplemental movie 2: 4D t(x,y,z,t) ime series (1 fpm) showing the recovery of the actin collar and hyphal tip growth after benomyl treatment and subsequent washout. Time is in hs:min

1405 Supplemental movie 3. Dual channel 4D acquisition (0.5 fpm) of nuclei/chromatin and F-actin/Lifeact. Time is in hs:min

Supplemental movie 4. 3D (x,y,t) series of GFP-actin acquired at 5 fps. Time is in sec:msec.

Supplemental movie 5. 3D (x,y,t) series of Lifeact-GFP acquired at 5 fps. Time is in
1410 sec:msec.

Supplemental movie 6. 3D time series of Lifeact-GFPat acquired at 5 fps, focusing on a peripheral actin filament revealing the formation of patches associated with it. Time is in sec:msec.

Supplemental movie 7. 3D time series (5 fps) of Lifeact-GFP that has been contrasted
1415 to reveal the presence of filamentous connections between patches. Time is in sec:msec.

Supplemental movie 8. 4D time series of Lifeact-GFP at 0.75 fps depicting ‘worms’ of F-actin moving basipetally. Time is in min:sec.

Supplemental movie 9. 4D time series of Lifeact-GFP filmed at 0.2 fps depicting ‘worms’ of F-actin moving basipetally and acropetally. Time is in min:sec.

1420 Supplemental movie 10. Three dimensional reconstitution of a z-stack of $AbpA^{Abp1}$-GFP hyphae.

Supplemental movie 11. Maximal intensity projection and individual optical sections of a deconvolved z-stack of Lifeact-GFP in an abortive *fimAΔ* germling.

Supplemental movie 12. Composition of 3D (x,y,t) movies (middle planes, 5 fps) depicting the behavior of F-actin patches in a *fimA::Tn341* hypha compared to the wild-type. Time is in sec:msec.

Supplemental movie 13. Three dimensional reconstruction of a z-stack of Lifeact-GFP in an abortive *cof1Δ* germling.

Supplemental movie 14. Behavior F-actin patches in a *srv2Δ* hyphal tip filmed with Lifeact-GFP at 5 fps. Time is in sec:msec.

Supplemental movie 15. Numerous actin worms in a *srv2Δ* cell filmed at 1 fps. Time is in min:sec.

Supplemental movie 16. Mutant *srv2Δ* tip with cortical patches giving rise to actin 'worms' that move away and towards the apex (on the right). 3D time series at 0.5 fps. Time is in min:sec.

Supplemental movie 17. A 'worm' apparently composed of two parallel filaments originates at an actin patch and moves basipetally. Lifeact-GFP photographed every 200 msec. Time is in sec:msec.

Supplemental movie 18. ArpC1-GFP filmed at 5 fps. Time is in sec:msec

Supplemental movie 19. ArpC1-mCherry and Vpr1-mCherry co-filmed at 0.2 fps. Time is in min:sec.

Supplemental movie 20. Time series representing a middle plane of a *capAΔ* hyphal tip cell expressing Lifeact-GFP. Acquired at 3 fps. Time in min:sec:msec.

Supplemental movie 21. Time series of Lifeact-GFP in *capAΔ abpAΔ* cells acquired at 10 fps. Time is in sec:msec.

Supplemental movie 22. Time series (1 fps) of a *dip1Δ* cell showing that actin cables arfe continuously being generated at the SPK. Time is in sec.

Supplemental movie 23. Time series (1 fps) showing conspicuous actin cables labeled with Lifeact-GFP in a *dip1Δ* cell. Time in min:sec.

Figure 1: A summary of the reporters used to detect F-actin structures

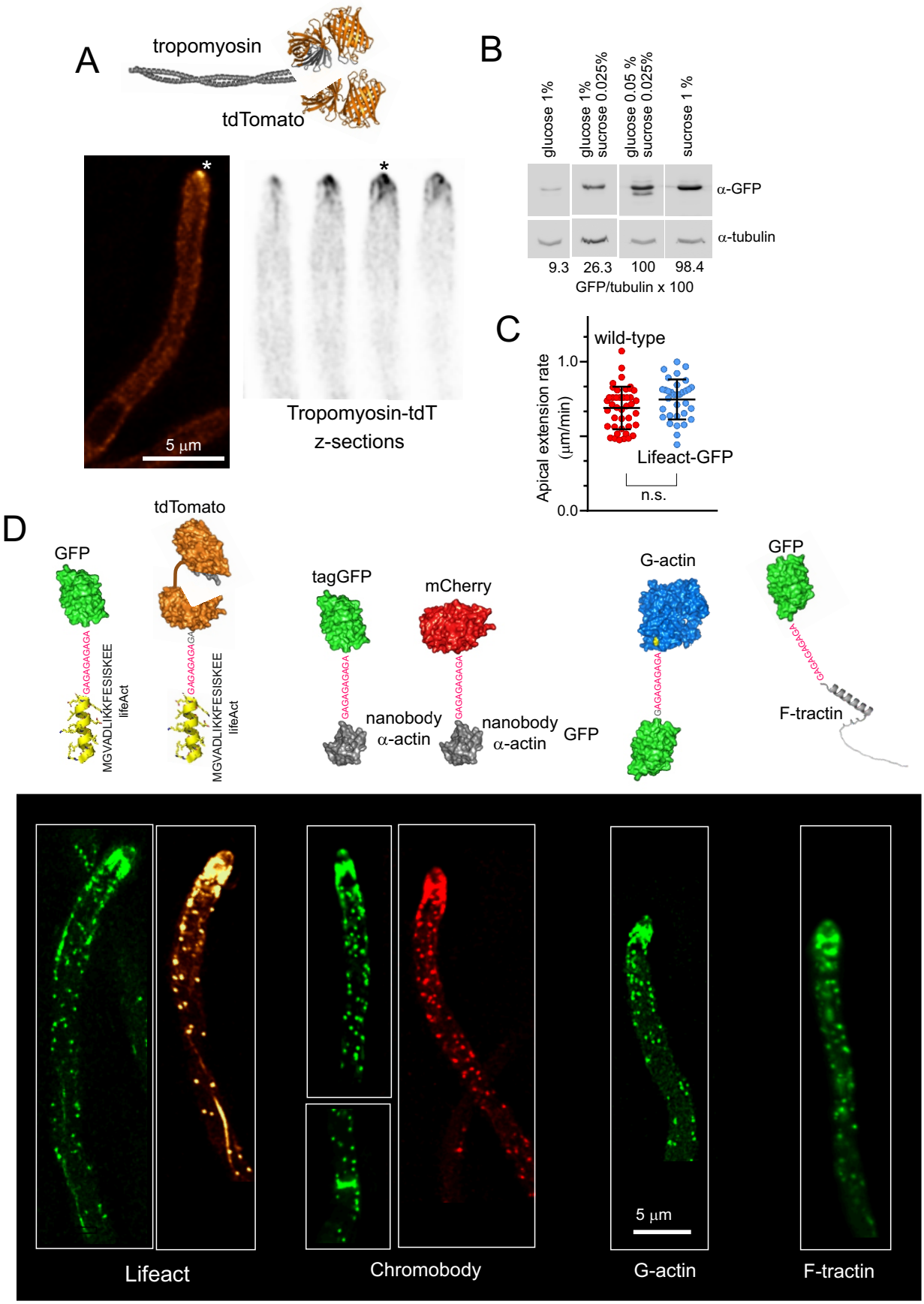

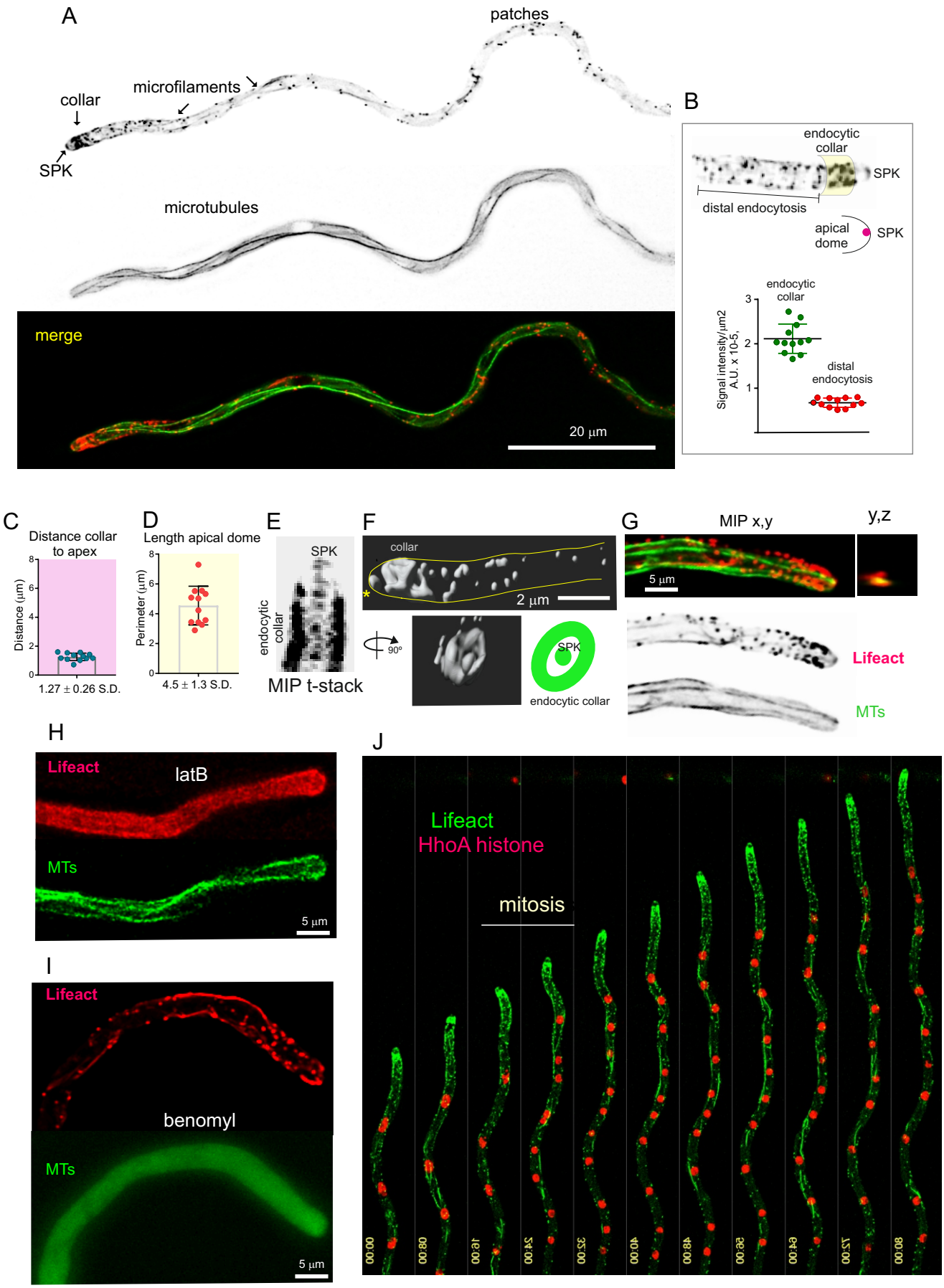

Figure 2. The actin cytoskeleton visualized with Lifeact

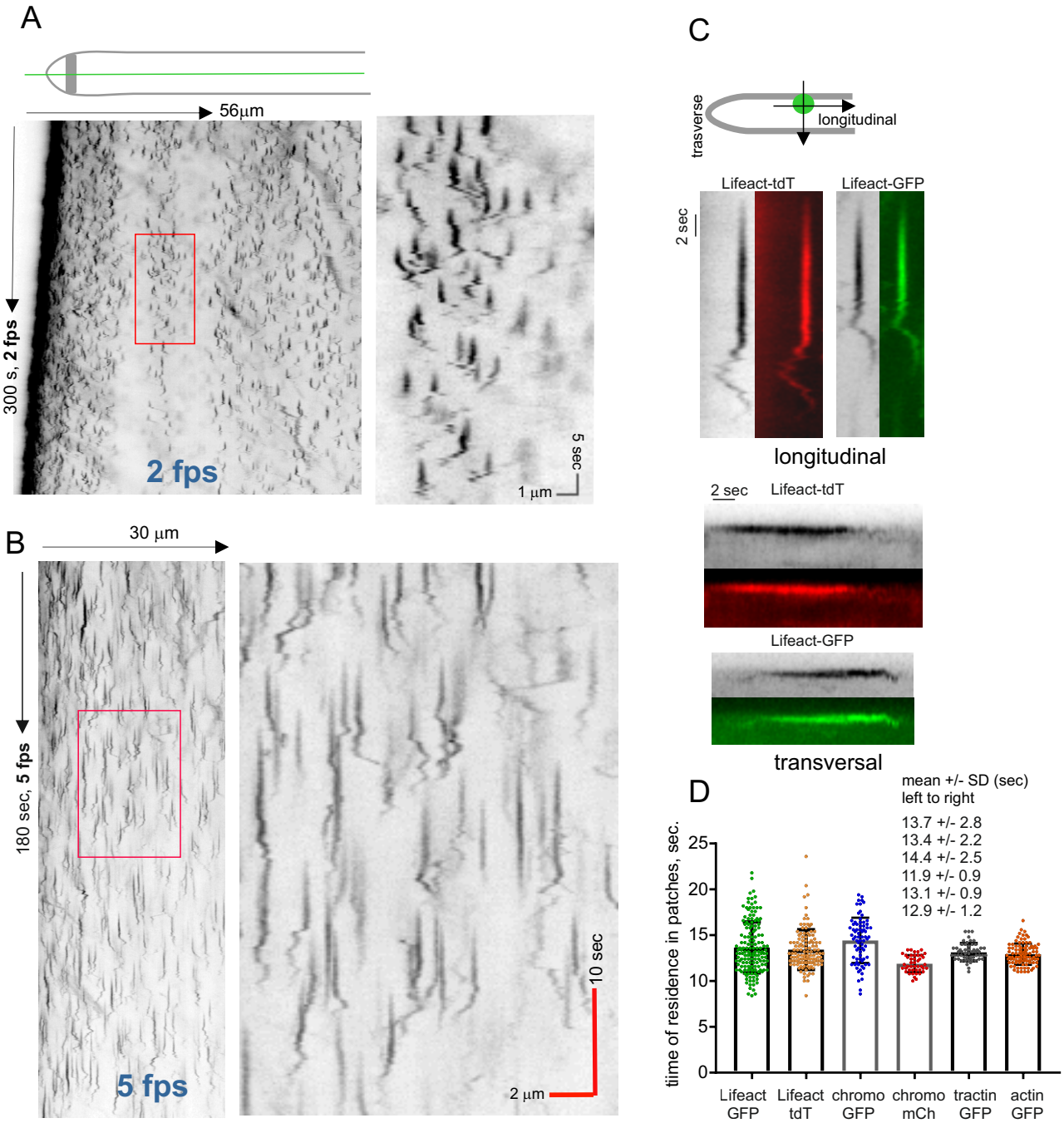

Figure 3. Determining the behavior and lifetime of actin patches visualized with F-actin reporters.

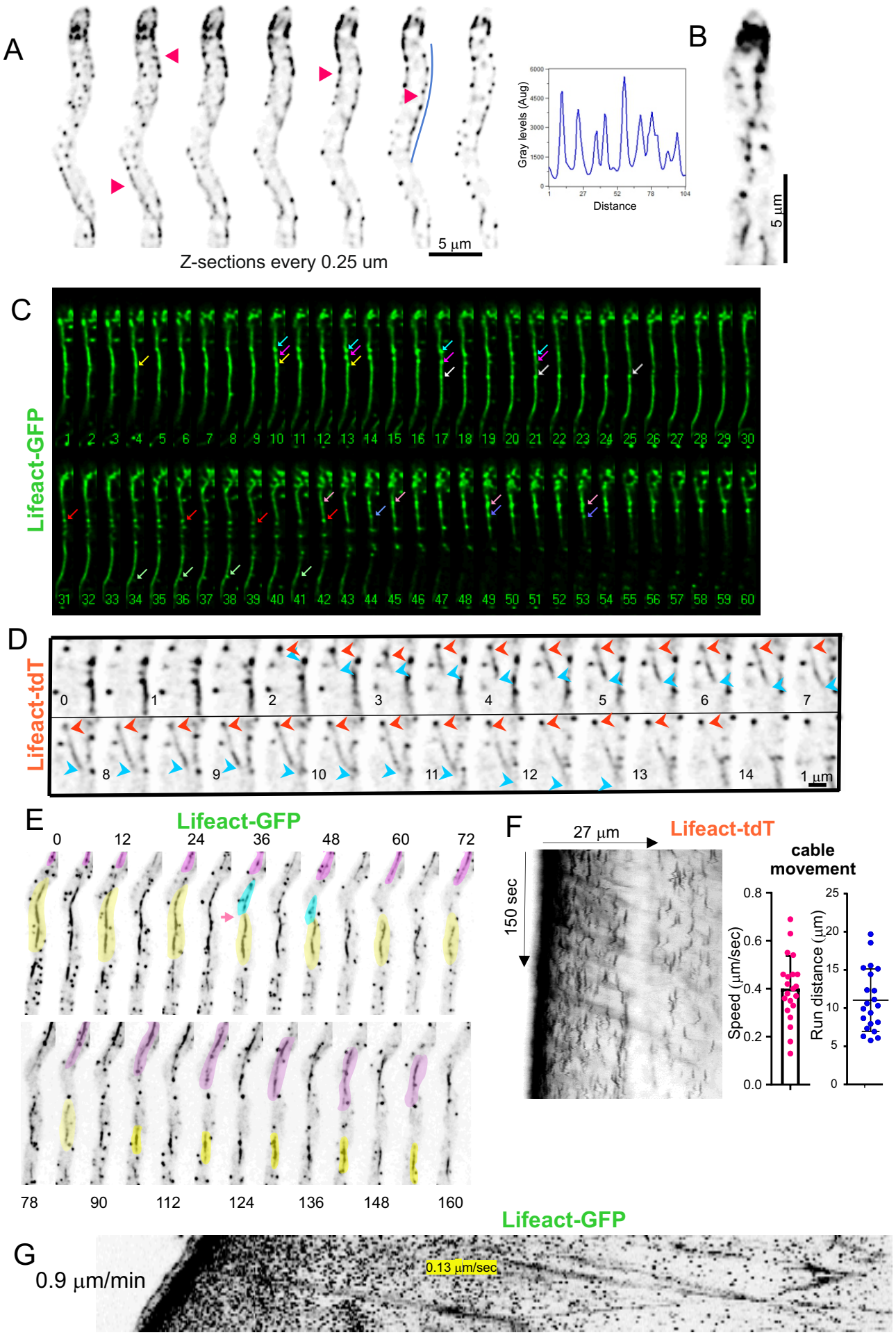

Figure 4. Actin patches associate with actin filaments

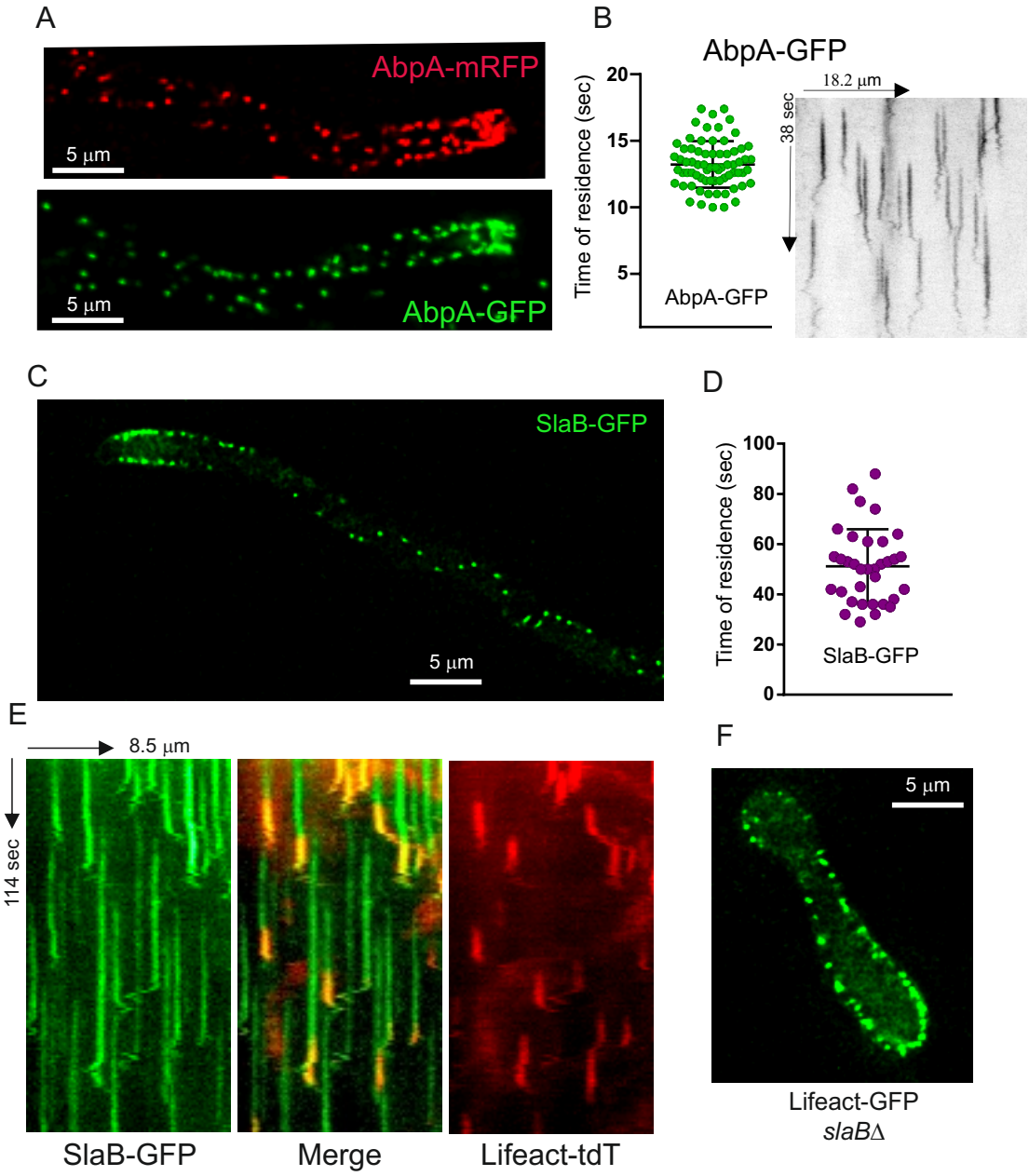

Figure 5. Localization and dynamics of AbpA^{Abp1} and SlaB^{Sla2}.

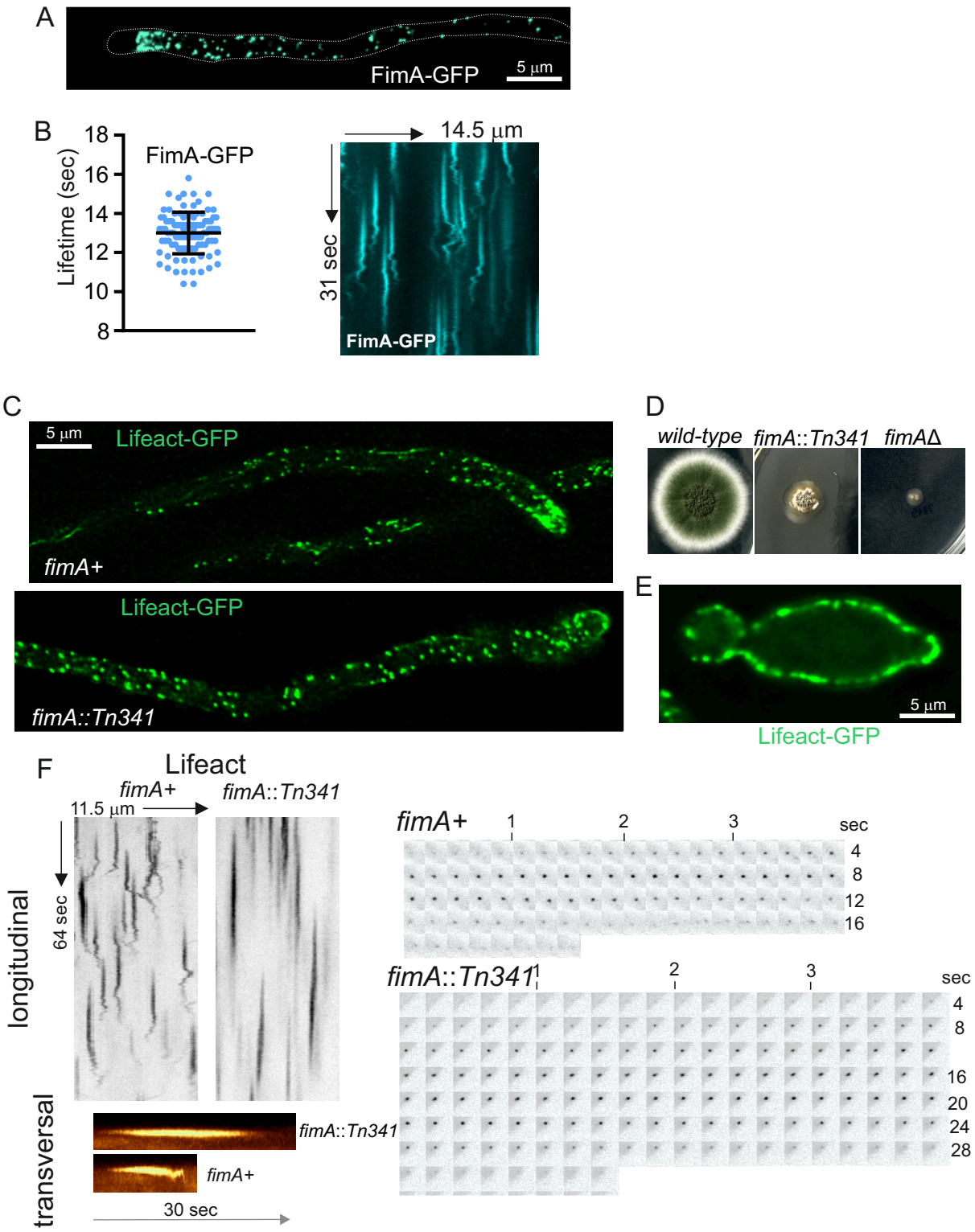

Figure 6. Localization and dynamics of fimbrin-GFP

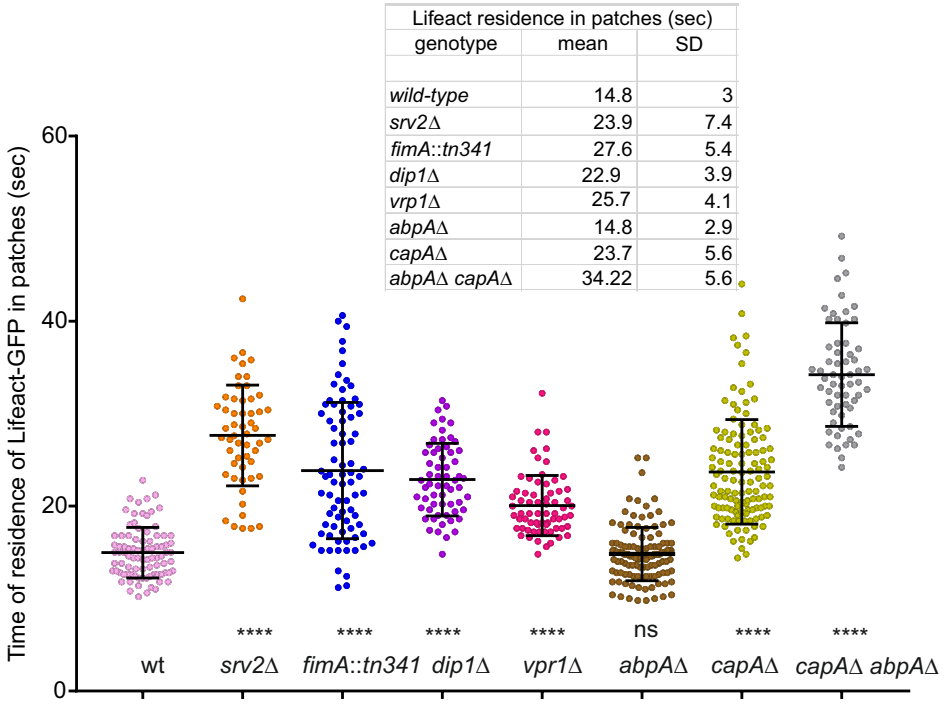

Lifeact residence in patches (sec)		
genotype	mean	SD
wild-type	14.8	3
srv2Δ	23.9	7.4
fimA::tn341	27.6	5.4
dip1Δ	22.9	3.9
vrp1Δ	25.7	4.1
abpAΔ	14.8	2.9
capAΔ	23.7	5.6
abpAΔ capAΔ	34.22	5.6

Figure 7. Lifeact-GFP patches in mutant backgrounds.

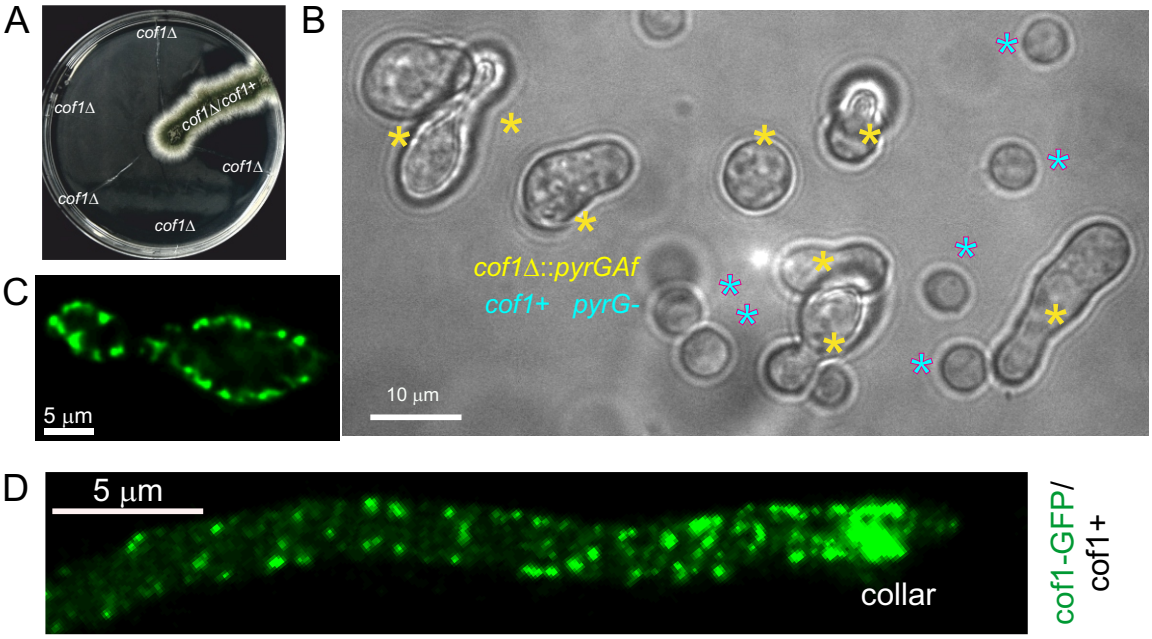

Figure 8. Cofilin is essential.

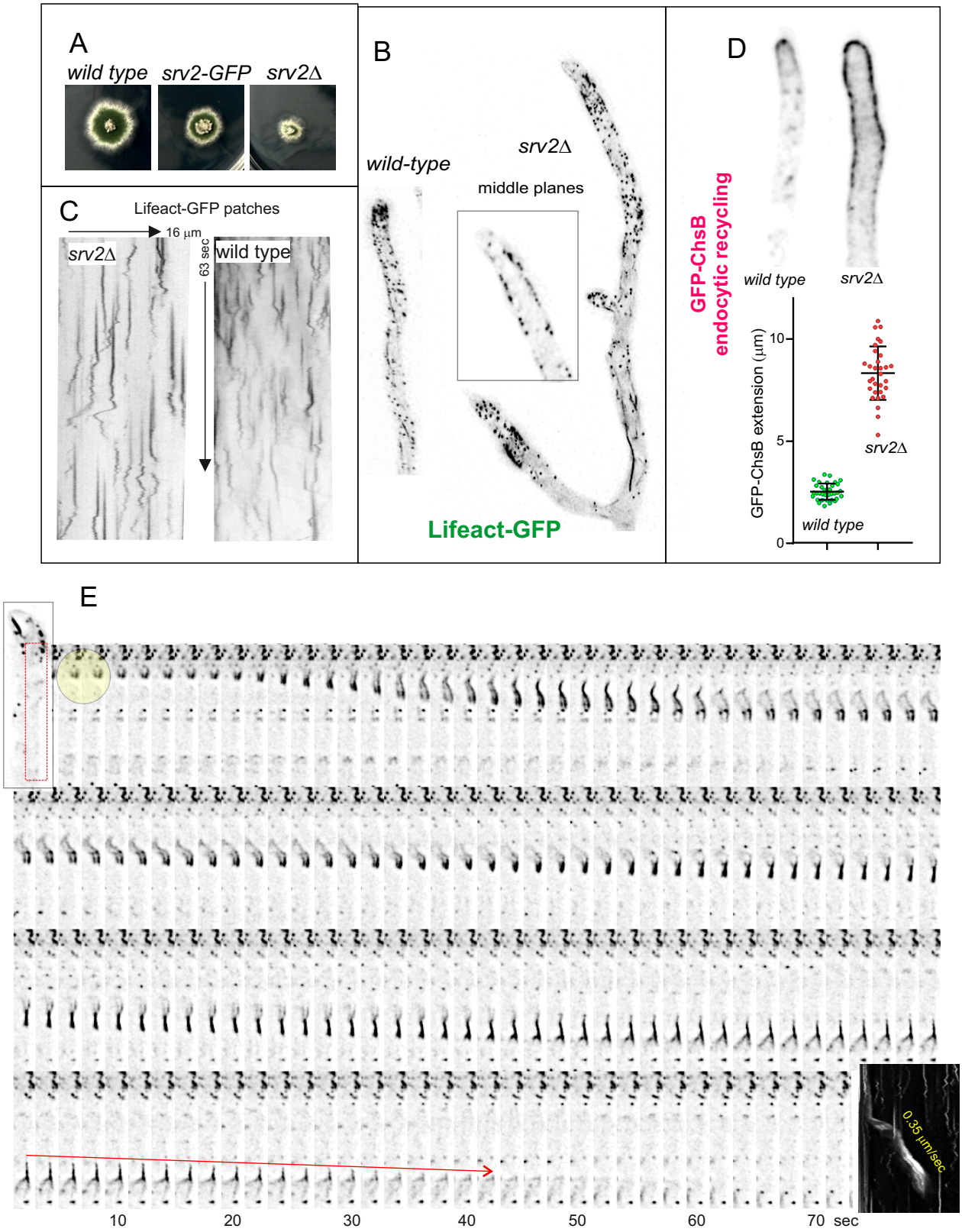

Figure 9. The role of Srv2/CAP in endocytosis.

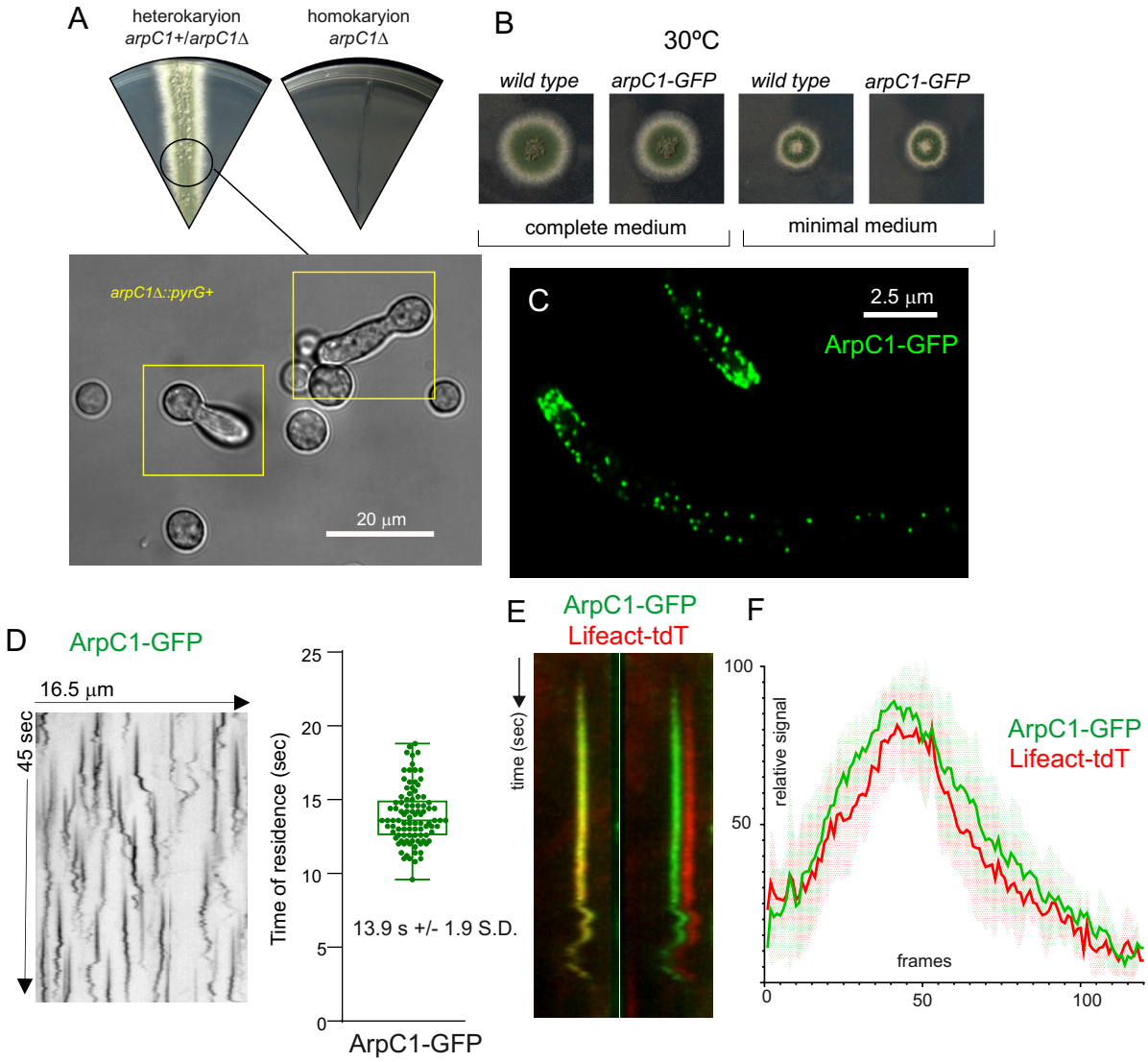

Figure 10. The Arp2/3 complex arrives at actin patches at roughly the same time than F-actin.

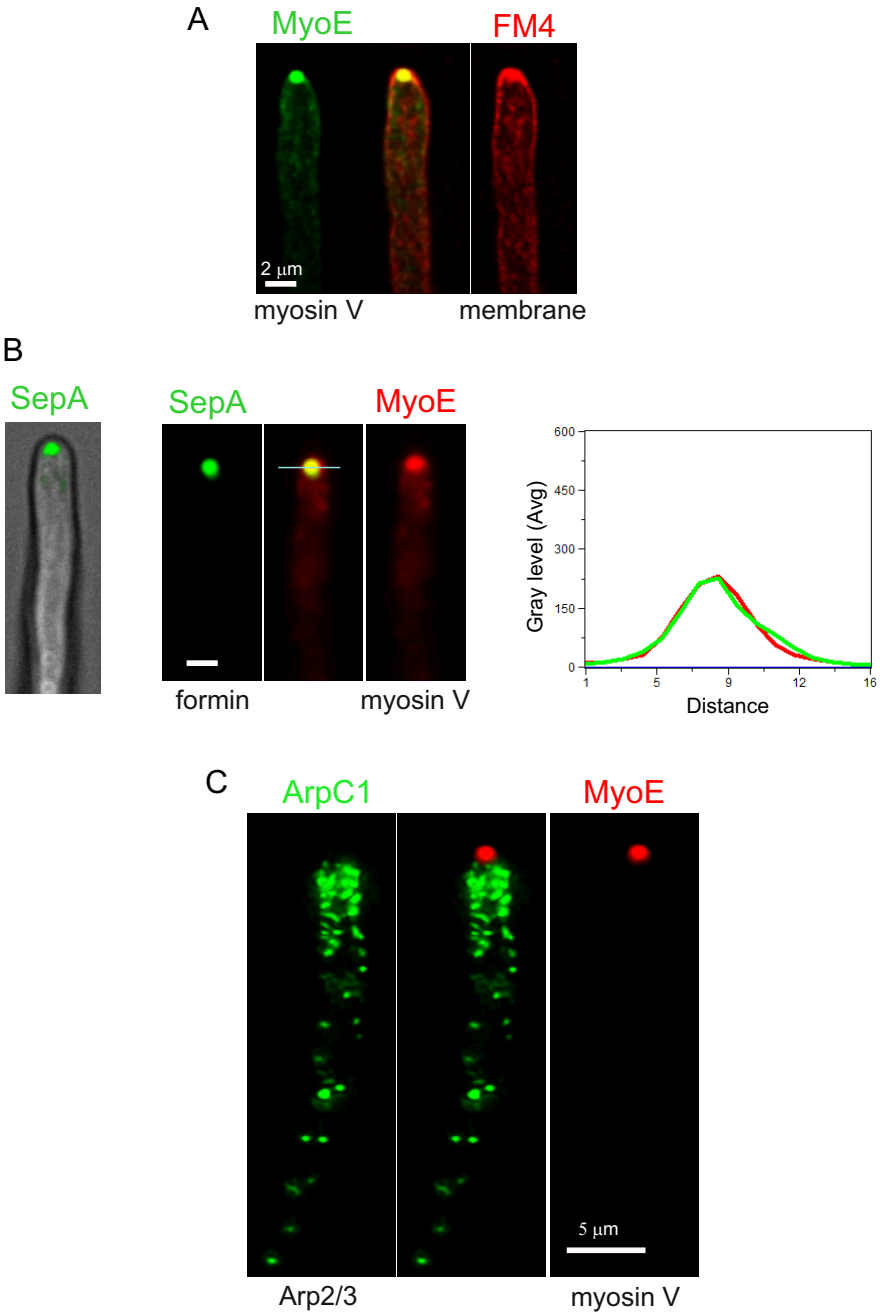

Figure 11. The Arp2/3 complex is excluded from the SPK

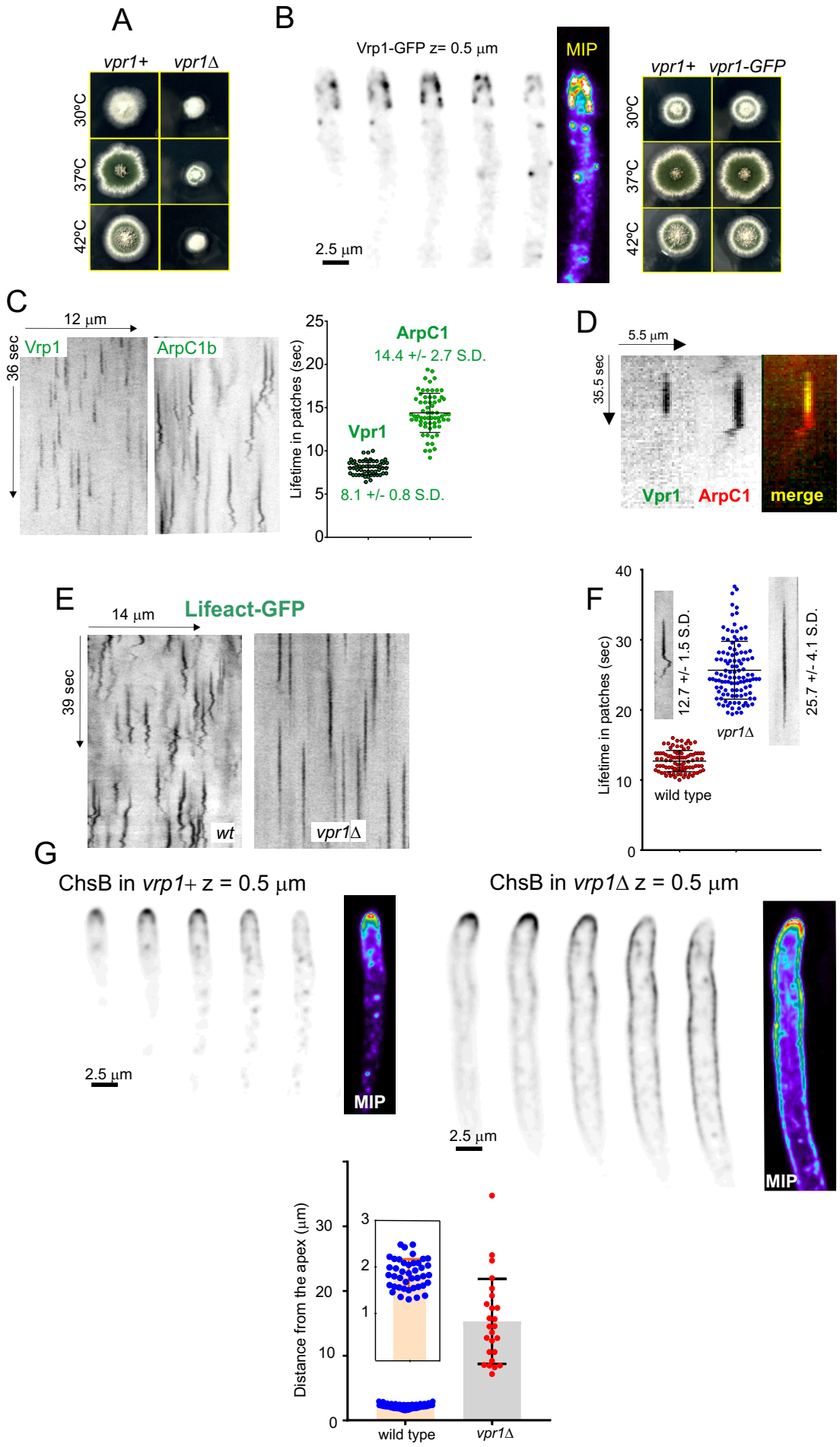

Figure 12. The motile phase of actin patches is dependent on Vpr1.

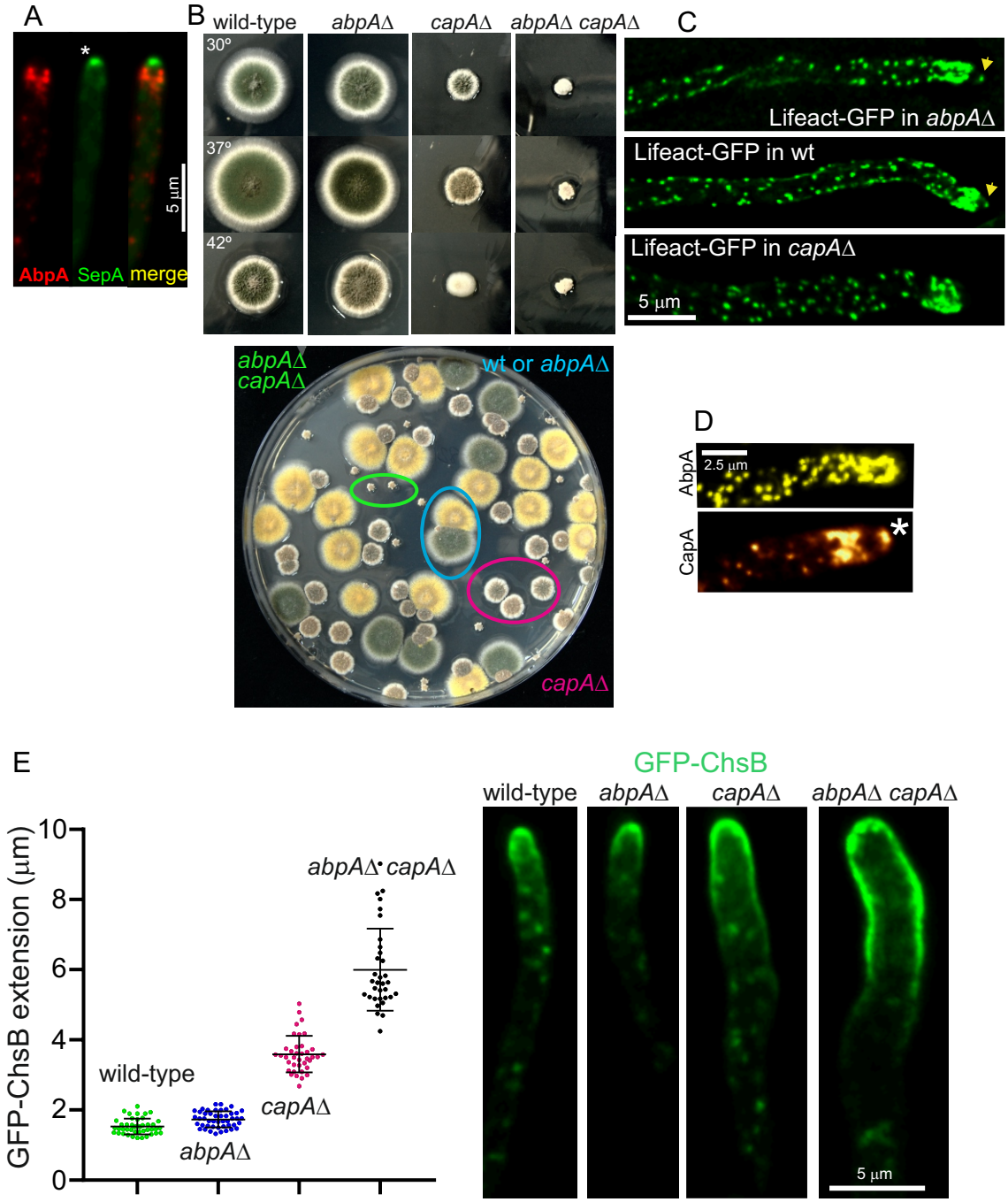

Figure 13. Synthetic negative interaction of *abpAΔ* and *capAΔ* mutants

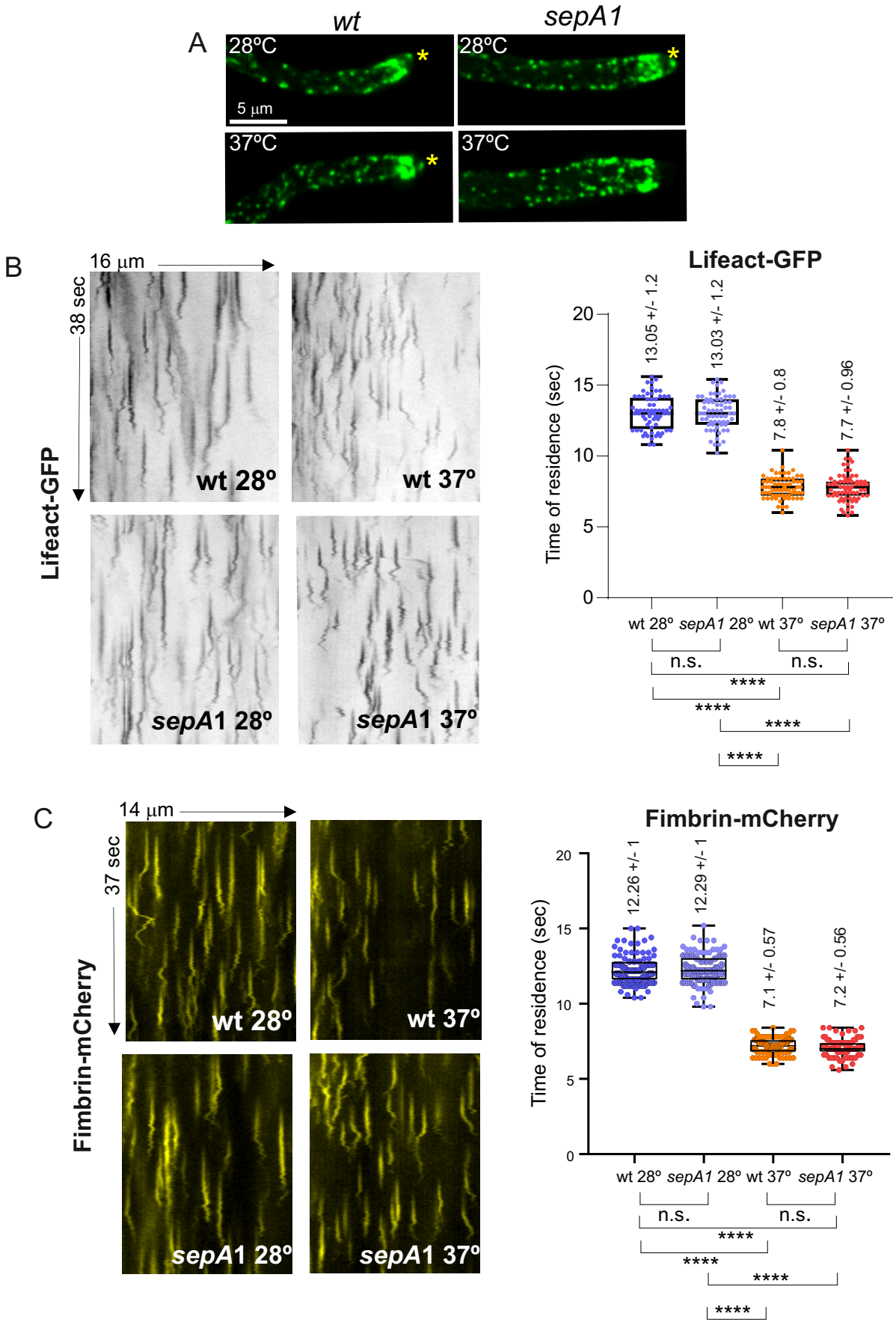

Figure 14. Conditional inactivation of formin does not affect the lifecycle of actin in patches

Figure 15. Dip1 is a key regulator of endocytic F-actin.

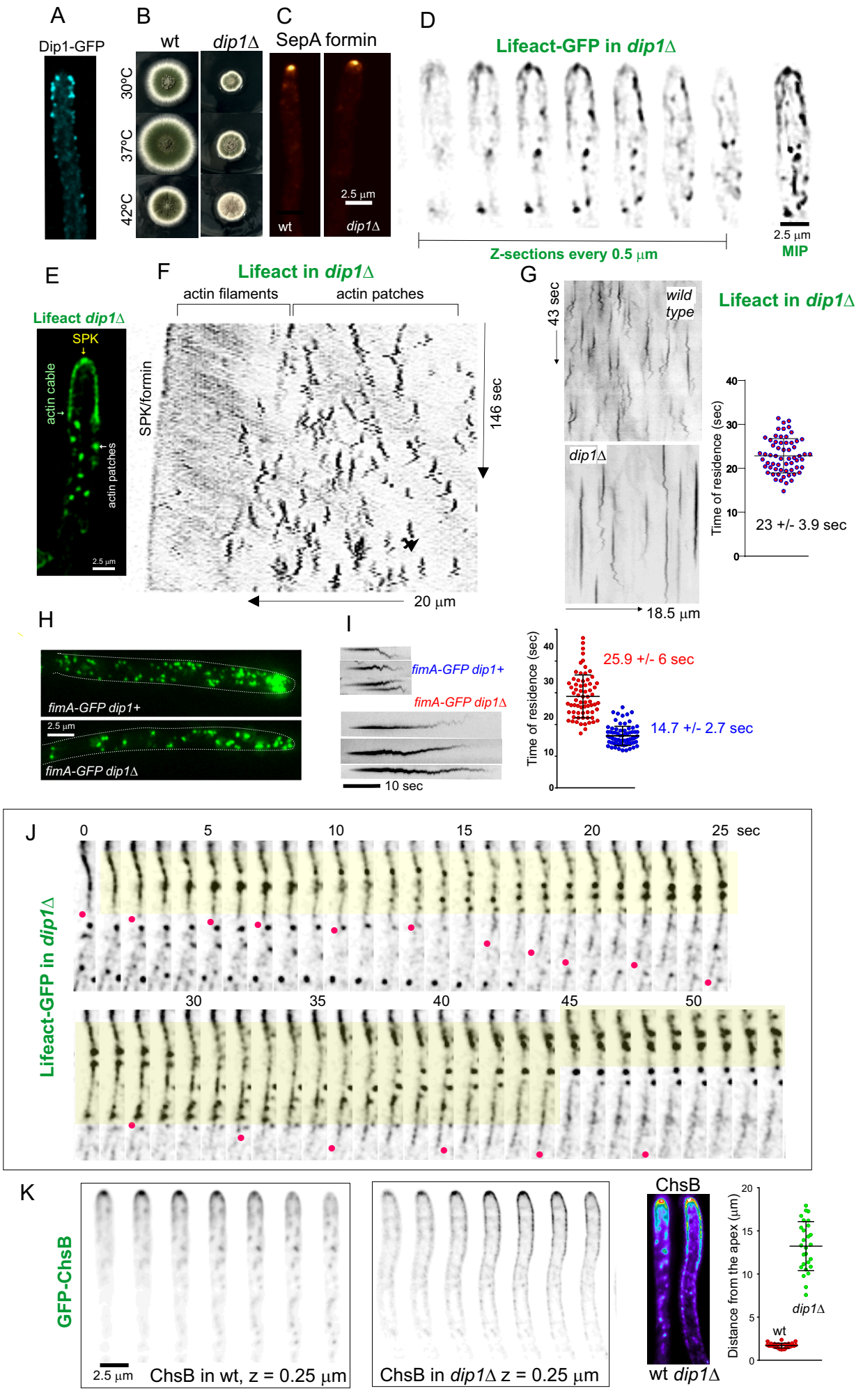

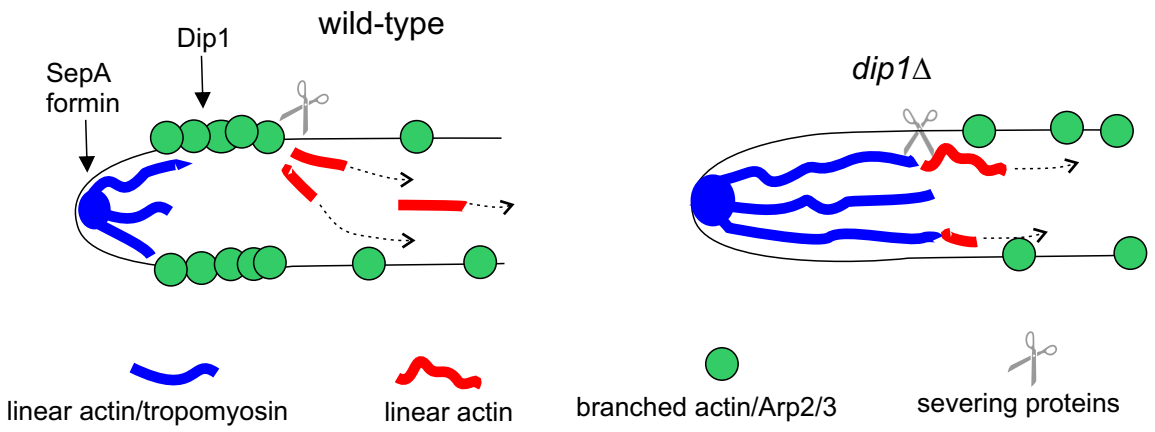

Figure 16. A model for the biogenesis of actin patches

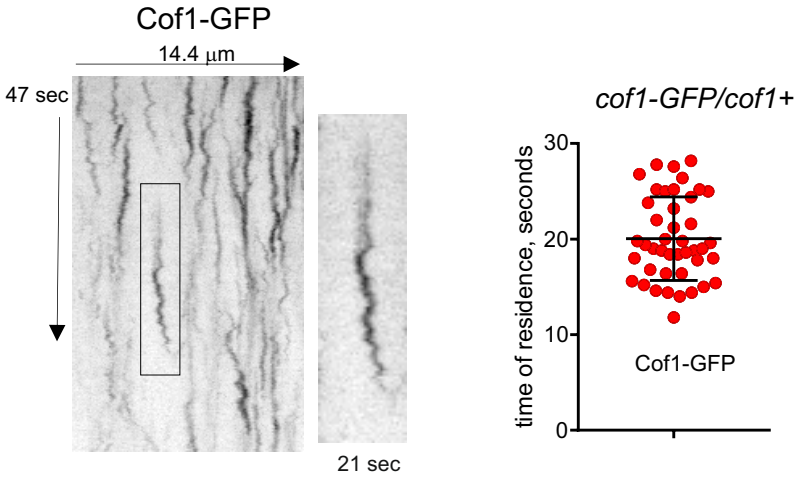

Supplemental Figure 1
Lifetime of Cof1-GFP in a strain containing a wild-type copy of the *cof1* gene to rescue viability, as endogenous tagging of Cof1 is lethal.

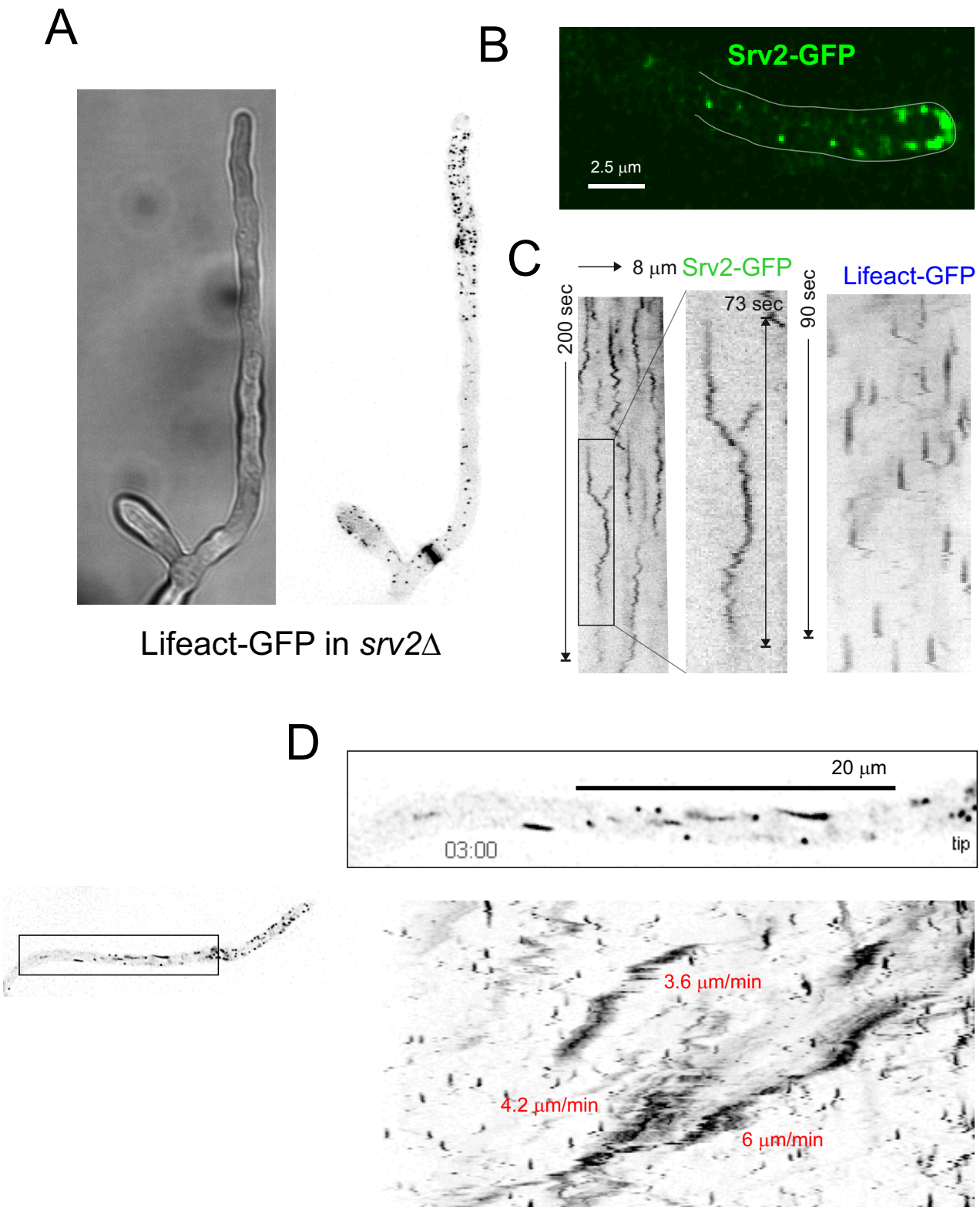

Supplemental Figure 2
(A) Ablation of Srv2 results in disorganization of the actin collar. (B) Localization of endogenously tagged Srv2-GFP. Note that the protein is not fully functional. Lifetime in actin patches of endogenously tagged Srv2-GFP and comparison with Lifeact-GFP patches in the wild-type. (D) "Worms" of F-actin moving towards the base of an *srv2Δ* strain, with a kymograph showing the corresponding speed

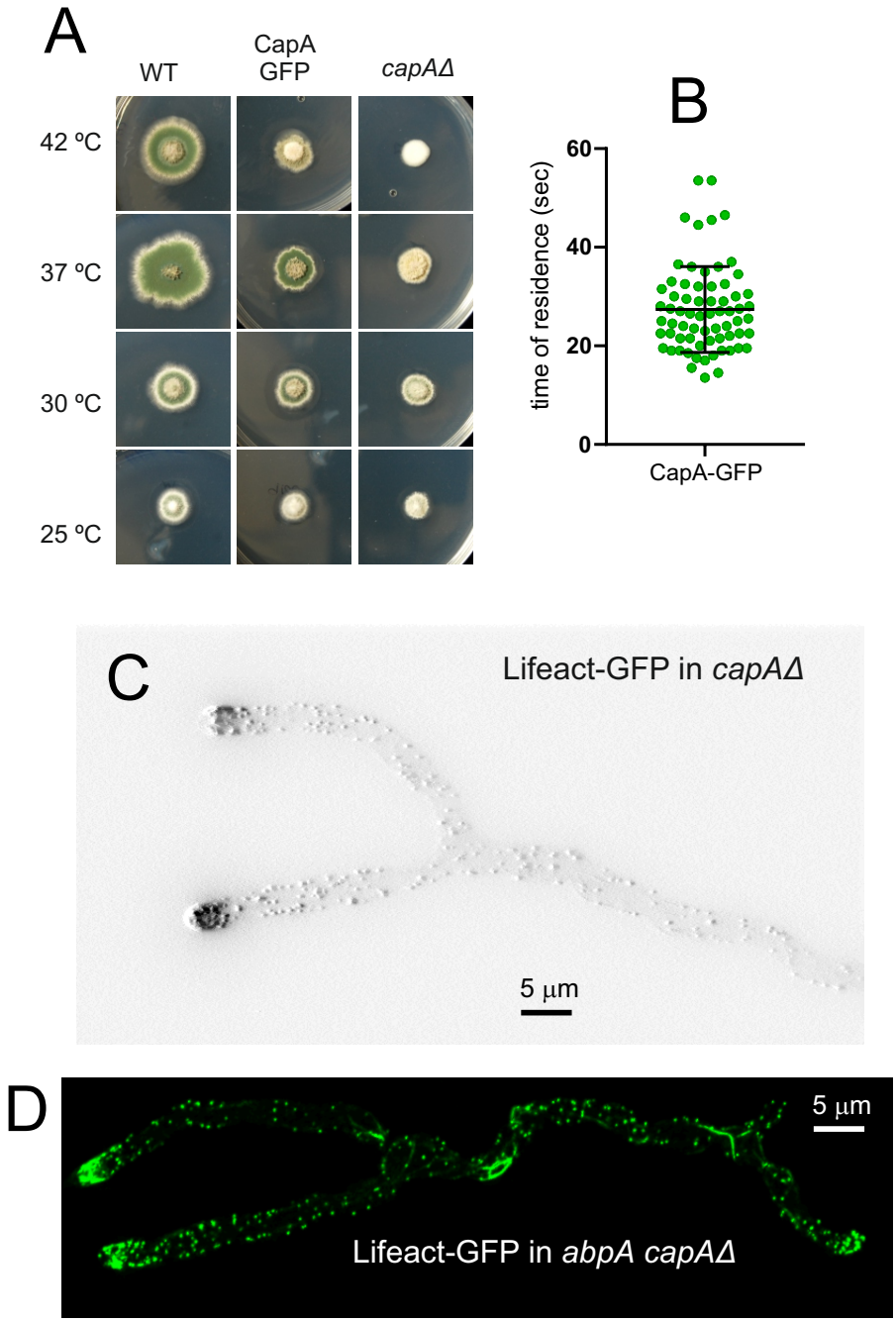

Supplemental Figure 3
(A) Growth tests comparing the wild-type with a strain expressing endogenously tagged CapA-GFP and the corresponding *capAΔ* deletion mutant, showing that CapA-GFP is only partially functional. (B) Average lifetime of CapA-GFP in cortical patches. (C) Split tip in a *capA*Δ strain expressing Lifeact-GFP. (D) Multiple polarity axes in an *abpA*Δ *capA*Δ double mutant cell expressing Lifeact-GFP.

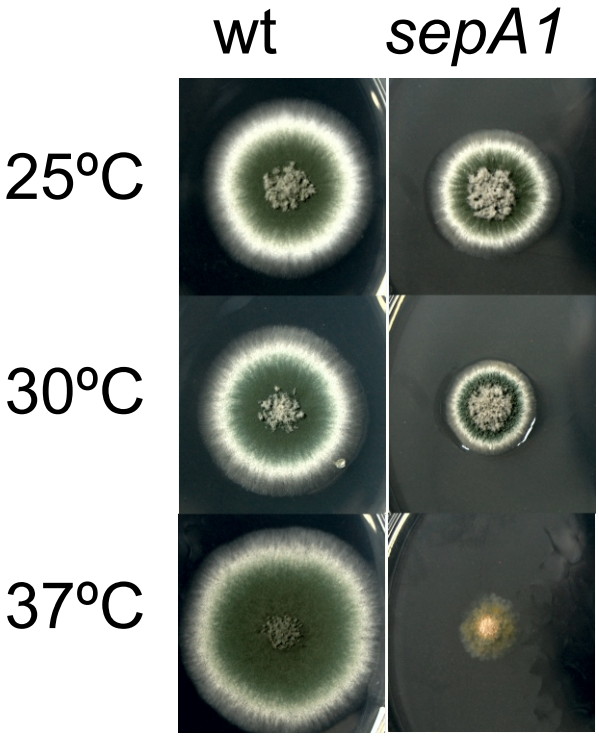

Supplemental Figure 4
sepA1 prevents growth at 37°C.

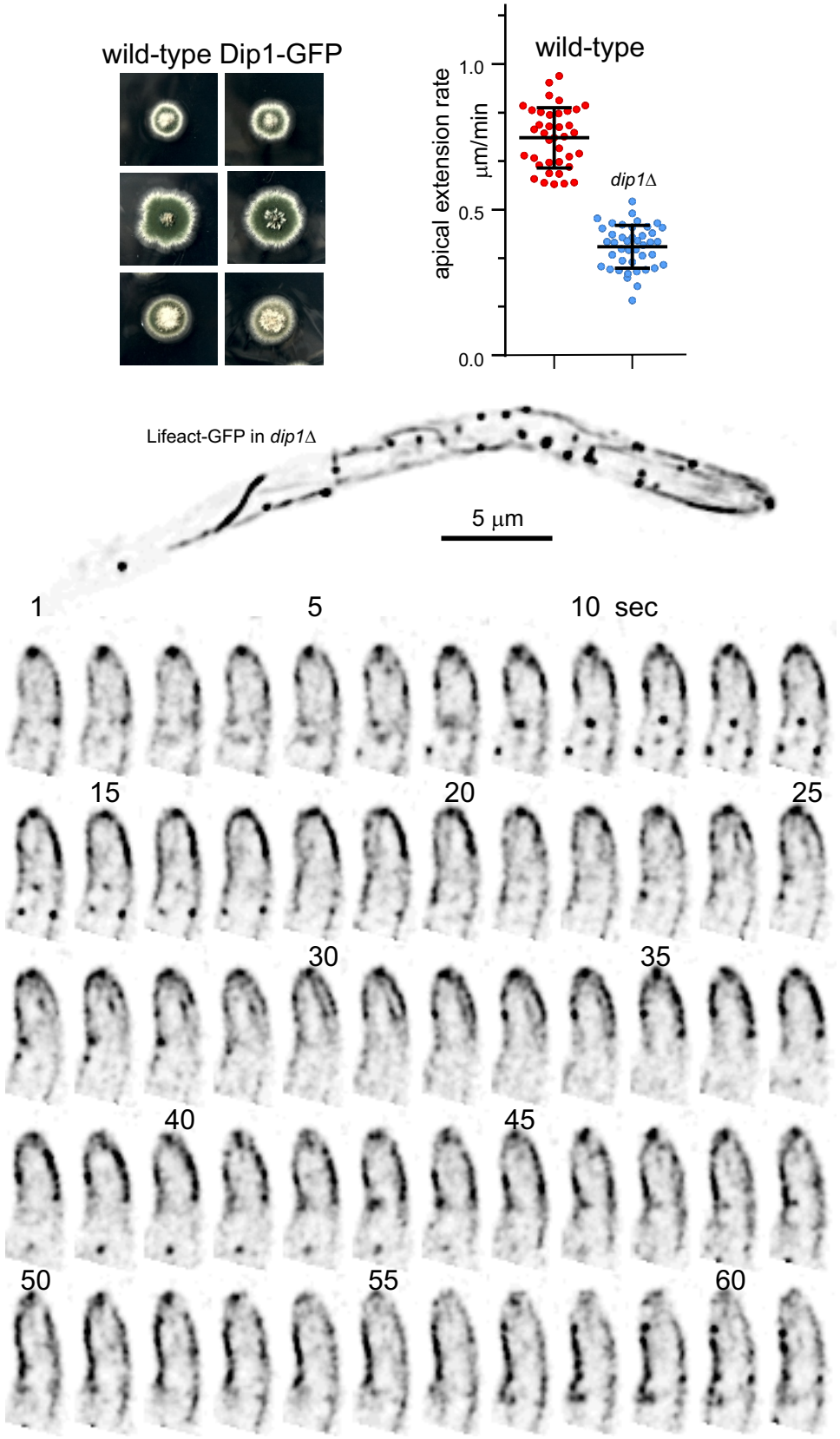

Supplemental Figure 5
(A) Growth test showing that Dip1-GFP is functional. (B) The apical extension rate of *dip1Δ* tips is half of the wild-type. (C) Deconvolved middle plane of a *dip1*Δ hypha expressing Lifeact-GFP. (D) Individual frames of a time-stack of a *dip1Δ* tip in which actin filaments emerge from the SPK.

Table S1: Strains used in this work

Strain code	Genotipe
MAD0002	*wt*
MAD1420	*yA2 pabaA1 pyrG89 abp1::gfp::pyrG*^{Af}
MAD1750	*pyrG89*; *wA3*; *pyroA4 tpmA*::gfp::*pyr4*
MAD1794	*pyrG89*; *argB2*; *pyroA4 nkuAΔ::argB; sla2::gfp::pyrG*^{Af}
MAD1802	*pyrG89*; *argB2*; *pyroA4 nkuAΔ::argB*; *abp1Δ::pyrG*^{Af}
MAD2294	*pabaA1 pyrG89?*; *abp1::rfp::pyrG*^{Af}
MAD4251	*fimA::Tn341::pyr4 pyrG89?*; *pyroA4 nkuAΔ::bar?*
MAD5321	*pyroA4 nkuAΔ::bar*; *riboB2*
MAD5851	*pyrG89*; *nkuAΔ::bar pyroA4*; *pyrG*^{Af}*::gfp::chsB*
MAD7134	*pabaA1*; *inuAp::lifeact::gfp::riboB*^{Af}*::inuAt*; *nkuAΔ::bar*; *riboB2*
MAD7183	*pyrG89; wA::tpmAp::tpmA::tdtomato::pyrG*^{Af}*::wA; pyroA4 nkuAΔ::bar*
MAD7209	*pabaA1*; *inuAp::lifeact::tdtomato::riboB*^{Af}*::inuAt*; *nkuAΔ::bar*; *riboB2*
MAD7259	*pabaA1*; *inuAp::lifeact::gfp::riboB*^{Af}*::inuAt*; *nkuAΔ::bar?*; *riboB2*; *hhoA*::rfp::*riboB*^{Af}
MAD7305	*inuAp::lifeact::tdtomato::riboB*^{Af}*::inuAt*; *nkuAΔ::bar?*; *slaB::gfp::pyrG*^{Af}
MAD7692	*pabaA1*; *wA::gfp::tubA::pyrG*^{Af}*::wA*; *inuAp::lifeact::tdtomato::riboB*^{Af}*::inuAt*; *nkuAΔ::bar?*
MAD7725	*inuAp::lifeact::gfp::riboB*^{Af}*::inuAt*; *pyroA4 nkuAΔ::bar?*; *slaB* 5'UTR::*pyrG*^{Af}*::niiAp::slaB*
MAD7727	*fimA::Tn341::pyr4*; *inuAp::lifeact::gfp::riboB*^{Af}*::inuAt*; *pyroA4 nkuAΔ::bar?*
MAD7729	*inuAp::lifeact::gfp::riboB*^{Af}*::inuAt*; *pyroA4 nkuAΔ::bar?*; *abp1Δ::pyrG*^{Af}
MAD7782	*pyrG89 yA2; argB2*::[*argB*::alcAp::mCherry::rabA*]; *nkuAΔ::argB*; *pantoB100 capAΔ::pyrG*^{Af}
MAD7815	*fimAΔ::pyrG*^{Af} *pyrG89*; *inuAp::lifeact::gfp::riboB*^{Af}*::inuAt*; *pyroA4 nkuAΔ::bar*; *riboB2*
MAD7820	*yA2 pyrG89?*; *inuAp::lifeact::gfp::riboB*^{Af}*::inuAt*; *nkuAΔ::bar?*; *pantoB100 capAΔ::pyrG*^{Af}; *riboB2?*
MAD7965	*pyrG89*; *pyroA4 nkuAΔ::bar*; *srv2Δ::pyrG*^{Af}
MAD7967	*pyrG89*; *pyroA4 nkuAΔ::bar*; *srv2::gfp::pyrG*^{Af}
MAD8062	*pyrG89? pabaA1; inuAp::lifeact::gfp::riboB*^{Af}*::InuAt; nkuAΔ::bar; srv2Δ::pyrG*^{Af} *riboB2*
MAD8082	*pyrG89; arpC1::gfp::pyrG*^{Af}; *pyroA4 nkuAΔ::bar*
MAD8125	*pyrG89 fimA::gfp::riboB*^{Af}*; pyroA4 nkuAΔ::bar; riboB2*
MAD8176	*pyrG89?*; *inuAp::lifeact::tdtomato::riboB*^{Af}*::inuAt*; *pyroA4 nkuAΔ::bar*; *arpC1::gfp::pyrG*^{Af}; *riboB2?*
MAD8181	*pyrG89*; *inuAp::gfp::actin::pyrG*^{Af}*::inuAt; pyroA4 nkuAΔ::bar*
MAD8184	*pyrG89 fimA::gfp::riboB*^{Af}; *pyroA4 nkuAΔ::bar*; *myoE::mcherry::pyrG*^{Af}; *riboB2*
MAD8186	*pyrG89?*; *myoE::mcherry::pyrGAf*; *nkuAΔ::bar*; *arpC1::gfp::pyrGAf*
MAD8301	*pabaA1*; *inuAp::actin-chromobody::tag-gfp::riboB*^{Af}*::inuAt; nkuAΔ::bar; riboB2*
MAD8303	*pabaA1*; *inuAp::actin-chromobody::mcherry::riboB*^{Af}*::inuAt; nkuAΔ::bar; riboB2*
MAD8559	*pabaA1 pyrG89*; *nkuAΔ::bar*; *cof1::gfp::pyrG*^{Af}*/cof1+*
MAD8641	*pyrG89 pabaA1*; *dip1Δ::pyrG*^{Af}*; nkuAΔ::bar*
MAD8643	*dip1Δ::pyrG*^{Af} *fimA::gfp::riboB*^{Af} *pyrG89*; *pyroA4 nkuAΔ::bar*; *riboB2*
MAD8726	*dip1Δ::pyrG*^{Af} *pyrG89 pabA1*; *nkuAΔ::bar*; *gfp::chsB::pyrG*^{Af}
MAD8728	*sepA::3xgfp::pyrG*^{Af} *pyrG89* pabaA1; *myoE::mCherry::pyrG*^{Af}; *pyroA4 nkuAΔ::bar*
MAD8736	*dip1Δ::pyrG*^{Af} *sepA*::3x*gfp::pyrG*^{Af} *pyrG89*; *pyroA4 nkuAΔ::bar*
MAD8761	*dip1::gfp::pyrG*^{Af} *pyrG89 pabaA1*; *nkuAΔ::bar*
MAD8809	*pyrG89*; *argB2*; *pyroA4 nkuAΔ::argB*; *abp1Δ::pyrG*^{Af} *capAΔ::pyrG*^{Af} *pantoB100*
MAD8810	*pyrG89*; *pyroA4 nkuAΔ::argB*; *capAΔ::pyrG*^{Af}
MAD8877	*inuAp::lifeact::gfp::riboB*^{Af}*::inuAt nkuAΔ::argB?*; *abp1Δ::pyrG*^{Af} *capAΔ::pyrG*^{Af}; *riboB2?*
MAD8917	*sepA1*; *inuAp::lifeact::gfp::riboBAf::inuAt*; *nkuAΔ::bar?*; *riboB2?*
MAD8939	*sepA1 fimA::mcherry::pyrG*^{Af} *pyrG89?*; *inuAp::lifeact::gfp::riboB*^{Af}*::InuAt*; *nkuAΔ::bar? riboB2?*
MAD8940	*fimA::mcherry::pyrG*^{Af} *pabaA1 pyrG89?*; *nkuAΔ::bar?*; *riboB2?*
MAD9025	*pabaA1 pyrG89?*; *pyroA4 nkuAΔ::bar?*; *pyrG*^{Af}*::gfp::chsB*; *srv2Δ::pyrG*^{Af}
MAD9049	*pyrG89*; *pyroA4 nkuAΔ::bar*; *vpr1Δ::pyrG*^{Af}
MAD9052	*pyrG89*; *pyroA4 nkuAΔ::bar?*; *capAΔ::pyrG*^{Af} *pyrG*^{Af}*::gfp::chsB*

Strain code	Genotipe
MAD9077	*pyrG*89; *pyroA*4 *nkuA*Δ::bar; *vpr1*::*gfp*::*pyrG*^{Af}
MAD9080	*pyrG*89; *inuA*p::*tractin-gfp*::*pyrG*^{Af}::*inuA*t; *pyroA*4 *nkuA*Δ::*bar*
MAD9083	*dip1*Δ::*pyrG*^{Af} *pyrG*89 *pabaA*1; *inuA*p::*lifeact*::*gfp*::*riboB*^{Af}::*inuA*t; *nkuA*Δ::*bar*; *riboB*2
MAD9085	*pyrG*89 *pabaA*1; *inuA*p::*lifeact*::*gfp*::*riboB*^{Af}::*inuAt; nkuA*Δ::*bar*; *riboB*2 *vpr1*Δ::*pyrG*^{Af}
MAD9089	*pyrG*89; *nkuA*Δ::*bar pyroA*4; *riboB*^{Af}::*gfp*::*chsB*; *vpr1*Δ::*pyrG*^{Af} *riboB*2
MAD9092	*pyrG*89; *pyroA*4 *nkuA*Δ::*bar*?; *abp1*Δ::*pyrG*^{Af} *pyrG*^{Af}::*gfp*::*chsB*
MAD9094	*pyrG*89; *pyroA*4 *nkuA*Δ::*bar*?; *capA*Δ::*pyrG*^{Af} *abp1*Δ::*pyrG*^{Af} *pyrG*^{Af}::*gfp*::*chsB*
MAD9100	*pyrG*89; *pyroA*4 *nkuA*Δ::*bar*; *capA*::*gfp*:*pyrG*^{Af}
MAD9296	*pyrG*89; *pyroA*4 *nkuA*Δ::*bar*; *arpC1*::*mcherry*::*pyroA*^{Af}; *vpr1*::*gfp*::*pyrG*^{Af}

Supplemental Table 2. Oligonucleotides used for genetic manipulation and plasmids constructions.

Primer name	**Sequence 5´-3´**
pGEM-T *inuA*p::*lifeact*::*gfp*::*riboBAf*::*inuA*t / *pGEM-T inuA*p::*lifeact*::*tdtomato*::*riboBAf*::*inuA*t	
Fw inuAp	GTGGAGGCCACTCTCGGAAAC
Rev InuAp join lifeact	CTCCTCCTTGGAGATGGACTCGAACTTCTTGATGAGGTCGGCGACGCCCATTTTGGTGATGTCGCTGACCGC
Fw GA5 join lifeact	ATGGGCGTCGCCGACCTCATCAAGAAGTTCGAGTCCATCTCCAAGGAGGAGGGAGCTGGTGCAGGCGCTGGAG
Fw inuAt join riboBAf	ACACGGTGTATGCTCGTCACACTCATAGGATCTAGCTAGATGTTTTGTTG
Rv RiboBAf	ATGAGTGTGACGAGCATACACC
Rv inuAt	CAGCAGTCAAGCAATACCAAGC
***inuA*p::*Actin-Chromobody*::*tag-gfp*::*riboBAf*::*inuA*t DNA cassette**	
Fw inuAp	GTGGAGGCCACTCTCGGAAAC
Rv inuAp join Actin-Chr-TagGFP	CAGACTCCACCAGCTGCACCTGAGCCATTTTGGTGATGTCGCTGACCGC
Fw Actin-Chr tagGFP join InuAp	TACGCGCGGTCAGCGACATCACCAAAATGGCTCAGGTGCAGCTGGTG
Fw RiboBAf join Actin-Chr-TagGFP	GCATGGACGAGCTGTACAGGTAAAAGAGGCCGTTCAGGAGTCTGG
Rv Tag-GFP join RiboBAf	CGAGCCAGACTCCTGAACGGCCTCTTTTACCTGTACAGCTCGTCCATGC
Rv RiboBAf join InuAt	CAACAAAACATCTAGCTAGATCCTCAGAACGTTTGCGCTGCAGAACCG
Fw InuAt join RiboBAf	GGTTCTGCAGCGCAAACGTTCTGAGGATCTAGCTAGATGTTTTGTTG
Rv InuAt	CAGCAGTCAAGCAATACCAAGC
***inuA*p::*Actin-Chromobody*::*mCherry*::*riboBAf*::*inuA*t DNA cassette**	
Fw inuAp	GTGGAGGCCACTCTCGGAAAC
Rv inuAp join Actin-Chr	CAGACTCCACCAGCTGCACCTGAGCCATTTTGGTGATGTCGCTGACCGC
Fw Actin-Chr join InuAp	TACGCGCGGTCAGCGACATCACCAAAATGGCTCAGGTGCAGCTGGTG
Rv Actin chr join mCherry	CGGCTCCAGCGCCTGCACCAGCTCCTGAGGAGACGGTGACCTGGGTC
Fw mChery join Actin Chr	GAGGGGACCCAGGTCACCGTCTCCTCAGGAGCTGGTGCAGGCGCTGGAG
Rv mCherry join RiboBAf	GCGGCATGGACGAGCTGTACAAGTAAAAGAGGCCGTTCAGGAGTCTGG
Rv RiboBAf join InuAt	CAACAAAACATCTAGCTAGATCCTCAGAACGTTTGCGCTGCAGAACCG
Fw InuAt join RiboBAf	GGTTCTGCAGCGCAAACGTTCTGAGGATCTAGCTAGATGTTTTGTTG
Rv InuAt	CAGCAGTCAAGCAATACCAAGC
***InuAp*::*Tractin*::*gfp*::*pyrGAf*::*inuA*t DNA cassette**	
Fw inuAp	GTGGAGGCCACTCTCGGAAAC
Rv Tractin join Gas-GFP::PyrGAf	CACCGGCTCCAGCGCCTGCACCAGCTCCGCCGGCAGCGGCAGCGGCAGC
Fw GAs-GFP::PyrGAf join Tractin	GCCGTCGCTGCCGCTGCCGCTGCCGGCGGAGCTGGTGCAGGCGCTGGAG
Rv PyrGaf join InuAt	AACAACAAAACATCTAGCTAGATCCTGTCTGAGAGGAGGCACTGATG
Fw inuAt join PyrGaf	ACGCATCAGTGCCTCCTCTCAGACAGGATCTAGCTAGATGTTTTGTTG
Rv InuAt	CAGCAGTCAAGCAATACCAAGC
***inuA*p::*gfp*::*Actin*::*pyrGAf*::*inuA*t DNA cassette**	
Fw inuAp	GTGGAGGCCACTCTCGGAAAC
Rv inuAp join GFP	CAGTGAAAAGTTCTTCTCCTTTACTCATTTTGGTGATGTCGCTGACCGC
Fw GFP join InuAp	CGCGCGGTCAGCGACATCACCAAAATGAGTAAAGGAGAAGAACTTTTC
Rv GAs GFP join Actin	GATAACGAGAGCAGCAACTTCCTCTTCCATGGCACCGGCTCCAGCGCCTG

Fw Actin join GAs GFP	CTGGTGCAGGCGCTGGAGCCGGTGCCATGGAAGAGGAAGTTGCTGCTC
Rv Actin Join PyrGAf	TCCAGCACACTGGCGGCCGTTACCTTGTATAACTAGCAATACTGTACTA
Fw pyrGAf Join Actin	TAGTACAGTATTGCTAGTTATACAAGGTAACGGCCGCCAGTGTGCTG
Rv PyrGaf join InuAt	AACAACAAAACATCTAGCTAGATCCTGTCTGAGAGGAGGCACTGATG
Fw inuAt join PyrGaf	ACGCATCAGTGCCTCCTCTCAGACAGGATCTAGCTAGATGTTTTGTTG
Rv InuAt	CAGCAGTCAAGCAATACCAAGC

***TpmA*::*tdTomato* cassette**

Fw wA 5´region	CGTCTATTGTAGAGCCTCCATGC
Rv wA 5´region join TpmA	GACATCTACTCGCTCTTGGATGACAAGTGATCAGGAGAAGGAGAGTCAAG
Fw TpmA Join wA 5´region	GCGGACTTGACTCTCCTTCTCCTGATCACTTGTCATCCAAGAGCGAGTAG
Rv TpmA join tdT::pyrGAf	CTATTCTAGGCGCGCCAACACTGTTCAAGGAGAGCTCG
Rv tdT::pyrGAf join wA 3´	GAAACGGGAAAGTAAAACCTTATGAGCGTCTGAGAGGAGGCACTGATG
Fw wA 3´region join pyrGAf	TCACGCATCAGTGCCTCCTCTCAGACGCTCATAAGGTTTTACTTTCCCG
Rv wA 3´region	CACCTGACTCGCATTGGAGAAC

***ArpC1::gfp* cassette**

Fw ORF *ARPC1*	CAGGCTCAACTGACTCTCATGC
Rev ORF *RPC1*	GATGGTCCAGATGACGACACGG
Fw join ORF *ARPC1 GFP-PyrG^{Af}*	GACGGCCGTGTCGTCATCTGGACCATCGGAGCTGGTGCAGGCGCTGGAG
Rv join 3UTR *ARPC1-pyrG^{Af}*	GTATGAAGCTCAGCCCAAGAACCAACGTCTGAGAGGAGGCACTGATG
Fw 3UTR *ARPC1*	GTTGGTTCTTGGGCTGAGCTTCAT
Rv 3UTR *ARPC1*	GGTGCATCGCCGTCAGTATCG

***ArpC1* Knock- Out cassette**

Fw 5UTR *ARPC1*	CCAGAAGGCTTTGGAGGCAAAGC
Rev 5UTR *ARPC1*	GTTGTTGTAAGGACAGGAGGAG
Fw join 5UTR *ARPC1-pyrG^{Af}*	GAGAGCTCCTCCTGTCCTTACAACAACGTAACGGCCGCCAGTGTGCTGG
Rv join 3UTR *ARPC1-pyrG^{Af}*	GTATGAAGCTCAGCCCAAGAACCAACGTCTGAGAGGAGGCACTGATG
Fw 3UTR *ARPC1*	GTTGGTTCTTGGGCTGAGCTTCAT
Rv 3UTR *ARPC1*	GGTGCATCGCCGTCAGTATCG

***sepA*::3x*gfp* cassette**

Fw *sepA* ORF	TTGGCTGCGTTCTTACAGGAG
Rv sepA ORF join GAs GFPs	CCGGCTCCAGCGCCTGCACCAGCTCCGCTGGTCGAGGGGCGATGTTC
Fw GAs GFPs join SepA	GATGATGAACATCGCCCCTCGACCAGCGGAGCTGGTGCAGGCGCTGGAG
Rv GFP join PyrGaf	CTTGTAGAGCTCGTCCATGCC
Fw PyrGAf	GCCTCAAACAATGCTCTTCACC
Rv PyrGAf join 3 UTR sepA	GGTAATAGGTCGGTGTGTGCGTCGGTCTGAGAGGAGGCACTGATG
Fw 3 UTR sepA join pyrGAf	CACGCATCAGTGCCTCCTCTCAGACCGACGCACACACCGACCTATTACC
Rv 3 UTR sepA	CTGCGAAGCATCGATGTTG

***Vpr1* Knock- Out cassette**

Fw 5UTR *VPR1*	GCGTGTGGACAATGCGGCAGAG
Rev 5UTR *VPR1*	GAGGGATCAGTAGAGATAGGG
Fw join 5UTR *VPR1-pyrG^{Af}*	ACCACGTCCCTATCTCTACTGATCCCTCGTAACGGCCGCCAGTGTGCTG
Rv join 3UTR *VPR1-pyrG^{Af}*	TTGTGGGTACAGTATCAATGCTAATAGGTCTGAGAGGAGGCACTGATG
Fw 3UTR *VPR1*	CTATTAGCATTGATACTGTACCC
Rv 3UTR *VPR1*	CAATTGCTTCATCCACTTCACC

***Vpr1*::*gfp* cassette**

Fw ORF *VPR1*	GTCGAGGAGGTGTTGATACTGG
Rev ORF *VPR1*	GCCGCTTAACGCGCTGAGATCC
Fw join ORF *VPR1 GFP-PyrG^{Af}*	GCCGTTGGATCTCAGCGCGTTAAGCGGCGGAGCTGGTGCAGGCGCTGGAG
Rv join 3UTR *VPR1-pyrG^{Af}*	TTGTGGGTACAGTATCAATGCTAATAGGTCTGAGAGGAGGCACTGATG
Fw 3UT *VPR1*	CTATTAGCATTGATACTGTACCC
Rv 3UTR *VPR1*	CAATTGCTTCATCCACTTCACC

***FimA* Knock- Out cassette**

Fw 5UTR *FIMA*	CGTTGTTACCGGACGCGGCTC
Rev 5UTR *FIMA*	CAGAATTTGGCTCCCCTCTCGC
Fw join 5UTR *FIMA -pyrG^{Af}*	GCCATTGCGAGAGGGGAGCCAAATTCTGGTAACGGCCGCCAGTGTGCTG
Rv join 3UTR *FIMA -pyrG^{Af}*	GTTCACAGGCTGCAGCCGTGAAGCGTCTGAGAGGAGGCACTGATG
Fw 3UTR *FIMA*	GCTTCACGGCTGCAGCCTGTG
Rv 3UTR *FIMA*	CATAGCAGCGGGAACGAGTGC

***Srv2* Knock- Out cassette**

Fw 5UTR *SRV2*	CGGTCCGTAACCATTCCATGC
Rev 5UTR *SRV2*	CTTGTCGGCTTTCTGGGCAGC
Fw join 5UTR *SRV2 -pyrG^{Af}*	GCCTCTGCTGCCCAGAAAGCCGACAAGGTAACGGCCGCCAGTGTGCTG
Rv join 3UTR *SRV2 -pyrG^{Af}*	AGGACAGGCCCAAAGTTAACGCCTGTGGTCTGAGAGGAGGCACTGATG
Fw 3UTR *SRV2*	CACAGGCGTTAACTTTGGGCCTGTC
Rv 3UTR *SRV2*	GTTGCCTCATACTAGCATAGAGATG

***Srv2*::*gfp* Cassette**

Fw OR *SRV2*	GGATGGAATAGATGCACAGGAGG
Rev ORF *SRV2*	GCCCGCATGCTCGACAATTTCG
Fw join ORF *SRV2 GFP-PyrG^{Af}*	GTCAGCGAAATTGTCGAGCATGCGGGCGGAGCTGGTGCAGGCGCTGGAG
Rv join 3UTR *SRV2 -pyrG^{Af}*	AGGACAGGCCCAAAGTTAACGCCTGTGGTCTGAGAGGAGGCACTGATG
Fw 3UTR *SRV2*	CACAGGCGTTAACTTTGGGCCTGTC
Rv 3UTR *SRV2*	GTTGCCTCATACTAGCATAGAGATG

***Dip1* Knock- Out cassette**

Fw 5UTR *DIP1*	GATGTTCCAGGCTGTCGACAAAG
Rev 5UTR *DIP1*	CCCACAACTCGGTCGTTGTCC
Fw join 5UTR *DIP1 -pyrG^{Af}*	GGCCCGAGGACAACGACCGAGTTGTGGGGTAACGGCCGCCAGTGTGCTG
Rv join 3UTR *DIP1 -pyrG^{Af}*	TGCCTCGACCAAACCCGCTCGTTTCGGGTCTGAGAGGAGGCACTGATG
Fw 3UTR *DIP1*	CCGAAACGAGCGGGTTTGGTC
Rv 3UTR *DIP1*	CAGTGAGACGCCATCAGTTACC

***Dip1*::*gfp* cassette**

Fw ORf *DIP1*	CAACAGTAGACGAAACCGCCTC
Rev ORF *DIP1*	GTGCAGCGAGACCTTCTGCAAAG
Fw join ORF *DIP1 GFP-PyrG^{Af}*	GAGGCTTTGCAGAAGGTCTCGCTGCACGGAGCTGGTGCAGGCGCTGGAG
Rv join 3UTR *DIP1 -pyrG^{Af}*	TGCCTCGACCAAACCCGCTCGTTTCGGGTCTGAGAGGAGGCACTGATG
Fw 3UTR *DIP1*	CCGAAACGAGCGGGTTTGGTC
Rv 3UTR *DIP1*	CAGTGAGACGCCATCAGTTACC

***CapA::gfp* cassette**

Fw ORF *CapA*	GAGGTGGGTTGTCGGTTCTACG

Rev ORF *CapA*	CCGCCCCTTTCCACCAGAGATATC
Fw join ORF *CapA GFP-PyrG*^{Af}	GGATATCTCTGGTGGAAAGGGGCGGGGAGCTGGTGCAGGCGCTGGAG
Rv join 3UTR *CapA -pyrG*^{Af}	CACAGAGAAAAACCACTGAGGTCCAGCGTCTGAGAGGAGGCACTGATGC
Fw 3UTR *CapA*	GCTGGACCTCAGTGGTTTTTCTCTG
Rv 3UTR *CapA*	GAGTCTGGTCAGGATACCGGAG

***CofA* Knock- Out cassette**

Fw 5UTR *COFA*	CTACTGGCCTTACCACTGTTTGC
Rev 5UTR *COFA*	GCAATATGTGATTTGCACTGGCAG
Fw join 5UTR *COFA -pyrG*^{Af}	GTCGTCTGCCAGTGCAAATCACATATTGCGTAACGGCCGCCAGTGTGCTG
Rv join 3UTR *COFA -pyrG*^{Af}	GGCCCGGACCCAGCCGTCGCCATTTGGTCTGAGAGGAGGCACTGATG
Fw 3UTR *COFA*	CAAATGGCGACGGCTGGGTCC
Rv 3UTR *COFA*	CTAGAGATAGTGCGGTAAGAGC

***Cof1::gfp* cassette**

Fw ORF *Cof1*	CGCATACATTGGAAATTCGTTCTG
Rev ORF *Cof1*	TTTGGCCTTACCACCGCTGACC
Fw join ORF *Cof1 GFP-PyrG*^{Af}	GCCGAGGTCAGCGGTGGTAAGGCCAAAGGAGCTGGTGCAGGCGCTGGAG
Rv join 3UTR *Cof1 -pyrG*^{Af}	GGCCCGGACCCAGCCGTCGCCATTTGGTCTGAGAGGAGGCACTGATG
Fw 3UTR *Cof1*	CAAATGGCGACGGCTGGGTCC
Rv 3UTR *Cof1*	CTAGAGATAGTGCGGTAAGAGC

***FimA::mCherry* cassette**

Fw ORF *FimA*	CAATGGCCGCGAAGGTAAGGCACC
Rev ORF*FimA*	CATTTTTTCGTACGTAGCCATTAGA
Fw join ORF *FimA* mCherry	TCTCTAATGGCTACGTACGAAAAAATGGGAGCTGGTGCAGGCGCTGGAG
Fw mCherry join *pyrG*^{Af}	GCGGCATGGACGAGCTGTACAAGTAAGTAACGGCCGCCAGTGTGCTG
Rv mCherry join *pyrG*^{Af}	GAATTCCAGCACACTGGCGGCCGTTACTTACTTGTACAGCTCGTCCATGC
Rv join 3UTR *FimA- pyrG*^{Af}	GTTCACAGGCTGCAGCCGTGAAGCGTCTGAGAGGAGGCACTGATG
Fw 3UTR *FimA*	GCTTCACGGCTGCAGCCTGTG
Rv 3UTR *FimA*	CATAGCAGCGGGAACGAGTGC

***FimA::gfp* cassette**

Fw ORF *FimA*	CAATGGCCGCGAAGGTAAGGCACC
Rev ORF *FimA*	CATTTTTTCGTACGTAGCCATTAGA
Fw join ORF *FimA GFP-RiboB*^{Af}	TCTCTAATGGCTACGTACGAAAAAATGGGAGCTGGTGCAGGCGCTGGAG
Rv join 3UTR *FimA -RiboB*^{Af}	GTTCACAGGCTGCAGCCGTGAAGCATGAGTGTGACGAGCATACACCGTG
Fw 3UTR *FimA*	GCTTCACGGCTGCAGCCTGTG
Rv 3UTR *FimA*	CATAGCAGCGGGAACGAGTGC